

pubs.acs.org/JPCC Article

Synthesis of $In_{1-x}Ga_xP$ Quantum Dots in Lewis Basic Molten Salts: The Effects of Surface Chemistry, Reaction Conditions, and Molten Salt Composition

Margaret H. Hudson,[§] Aritrajit Gupta,[§] Vishwas Srivastava, Eric M. Janke, and Dmitri V. Talapin*



Cite This: J. Phys. Chem. C 2022, 126, 1564–1580



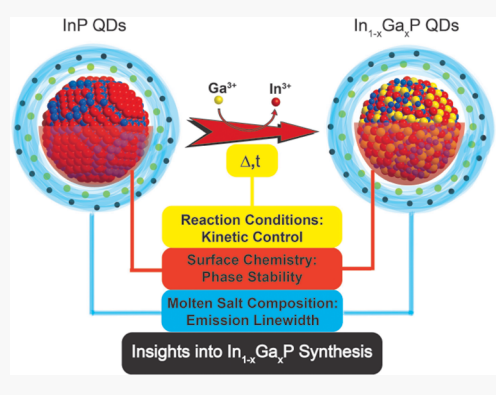
ACCESS

Metrics & More

Article Recommendations

Supporting Information

ABSTRACT: Inorganic molten salts are emerging as versatile solvents for high-temperature processing of colloidal nanocrystals. Molten alkali bromide eutectics can serve as a convenient solvent for the transformation of InP quantum dots (QDs) to $In_{1-x}Ga_xP$ QDs, with simultaneous tuning of the composition and band gap. Here, we explore various aspects of this molten salt indium-to-gallium cation exchange in-depth, including the nanocrystal surface chemistry, reaction conditions, and salt composition, to obtain a more detailed understanding and finer control over the transformation. InP QDs capped with (DDA)₂S, (NH₄)₂S, $Inclate{Li}_2$ Se, $Inclate{Ga}_3$ Se, $Inclate{Ga}_3$ Se, $Inclate{Ga}_3$ Se, $Inclate{Ga}_3$ Se demonstrate that chalcogenide capping ligands improve the high temperature stability of InP QDs through the formation of a chalcogen-rich layer which prevents InP decomposition. For each surface chemistry studied, the indium-to-gallium cation exchange proceeds similarly, yielding colloidal $Inlate{Ga}_3$ P



QDs with an increased band gap and decreased lattice constant. By carefully engineering the reaction conditions and protecting the nanoparticles from oxidative exposure, we achieve a narrow emission linewidth of 41 nm full width at half maximum from the alloyed $In_{1-x}Ga_xP$ colloidal QDs. These insights provide the design space for colloidal synthesis in molten inorganic salts and introduce synthetic methods for $In_{1-x}Ga_xP$ QDs with tunable composition and properties. Our work demonstrates the development of nontoxic QD emitters with optimized stability, color purity, and luminescence quantum efficiency.

INTRODUCTION

Much effort has been devoted to the development of colloidal quantum dots (QDs) as tunable emitters with narrow emission linewidths for applications as phosphors or emissive layers in display technologies.^{1,2} The field has been initially dominated by the optimization of CdSe QDs, whose high brightness with ~100% quantum yield (QY) and narrow emission spectra (~20-30 nm full width at half maximum, FWHM) outperform the characteristics of organic dyes and other solutionprocessed emitters.^{3,4} However, toxicity concerns for materials used in consumer electronics have inspired the development of nontoxic alternatives to CdSe QDs. 5,6 Heavy-metal-free InP QDs have emerged as a strong competitor to CdSe for applications in tunable visible light emission.^{2,7,8} InP QDs have achieved high brightness (>90% QY) and narrow linewidths (35 nm),^{9,10} but their performance still lags behind that of CdSe QDs due to several synthetic and structural problems. The covalent character of the InP lattice and the high reactivity of its synthetic precursors make the optimization of synthetic protocols difficult. 11,12 Moreover, the InP phase is highly susceptible to oxidation. 13,14 Despite these challenges, high performance InP emitters have been developed through advanced core synthesis followed by the growth of successive ZnSe and ZnS shells to yield bright, stable materials. 9,10,15,16

Yet recent work has shown that unintentional zinc-doping of the InP core creates emissive in-gap states which broaden the ensemble photoluminescence (PL). In traditional optoelectronic devices utilizing III—V semiconductors, such heterovalent doping is avoided by using lattice-matched, alloyed III—V materials as wide band gap passivating layers. The synthesis of sophisticated all-III—V core/shell nanocrystals (NCs) is yet to be achieved with colloidal synthetic methods; however, there has been some initial success in the colloidal synthesis of InP/GaP/ZnS^{7,20} and InZnP/InGaP/ZnSeS²¹ heterostructures with high QYs (>70%).

We introduced molten salt processing as a method to overcome several persistent problems in III—V QD materials synthesis. ^{22,23} Molten inorganic salts are robust, high temperature solvents with a wide electrochemical window, making them an inert matrix for many synthetic transformations. Recent work has shown that NCs can be dispersed in a variety

Received: December 7, 2021 Revised: December 23, 2021 Published: January 14, 2022





of molten salts.^{24,25} Specific chemical interactions between the NC surface and the salt matrix induce structuring of the molten salt ions around the NCs which prevents direct contact of the NC surfaces. Thus, NCs can be dispersed throughout the salt matrix and protected from sintering. In addition, alkali halide melts are rigorously oxygen free and have recently been used to synthesize a variety of oxidation prone ceramic materials directly in air.²⁶ These conditions are ideal for synthetic transformations of III–V QDs.

Recently, a method has been developed for the synthesis of III-V alloy QDs in an alkali halide molten salt matrix.²³ InP or InAs QDs synthesized by traditional colloidal synthesis can be dispersed in a molten inorganic salt and transformed to In_{1-x}Ga_xP or In_{1-x}Ga_xAs alloyed QDs by annealing in the presence of Ga³⁺ at 380–450 °C. This cation exchange produces colloidal QDs with a wider band gap and reduced lattice constant. Thermodynamic analysis of this cation exchange reaction shows that GaP ($\Delta H_{\rm f,298\it K}^0 = -100.1~{
m kJ/}$ mol) is a significantly more stable phase than InP ($\Delta H_{\rm f,298K}^0 = -61.6$ kJ/mol), and the reaction is energetically favorable.²⁷ The InP to In_{1-x}Ga_xP cation exchange introduces several new properties which may be advantageous for technological applications: higher extinction coefficient, better lattice match with wide band gap ZnS shells, and improved high temperature PL.²³ Moreover, the indium-to-gallium cation exchange produces a phase with improved temperature stability; at any given temperature, the partial pressure of phosphorus above InP is higher than that above GaP.²⁷

In this manuscript, we aim to systematically investigate and better understand the molten salt chemistry of colloidal nanomaterials. The molten salt synthesis of In_{1-x}Ga_xP QDs still needs to be optimized to further improve the optical properties. Surface chemistry dictates the interaction between the OD surface and the molten salt matrix; thus, the choice of surface chemistry may impact the dispersion of the QDs within the salt, ^{24,25} the thermodynamic favorability of cation exchange at the QD surface,²⁸ and the stability of the nanocrystalline III-V phase.²⁹⁻³¹ Designing synthetic conditions that stabilize the QD lattice should prevent the formation of crystalline defects and impede broadening of the size distribution through ripening, improving the emission QY and linewidth, respectively. Additionally, tuning the cation exchange to achieve a breadth of alloy compositions ($In_{1-x}Ga_xP$, where x = 0-1) with control over cation distribution within the QD lattice would allow us to achieve novel nanostructures which mimic well-developed epitaxial structures. For instance, the creation of all-III-V core shells may improve the emission QY without the inclusion of heterovalent ions. To attain control over the cation exchange reaction, we seek to understand its mechanism through variations in the temperature and time of reaction as well as changes in composition of the molten salt reaction medium. Knowledge gained though our extensive studies on the influence of surface chemistry and reaction conditions on the molten salt indium-to-gallium cation exchange has allowed us to achieve a narrow emission linewidth of 41 nm (0.16 eV) from an optimized synthesis of the colloidal alloyed III-V QDs.

EXPERIMENTAL SECTION

All experiments were performed in a nitrogen glovebox with <2 ppm oxygen and moisture, unless otherwise noted.

Materials. Hexamethylphosphoramide (HMPA, 99%), trioctylphosphine (TOP, 97%), ammonium sulfide (40–48

wt % in water), didodecyldimethylammonium bromide (DDAB, 98%), trioctylphosphine oxide (TOPO, 99%), hydrofluoric acid (HF, 48 wt % in water), and anhydrous solvents (hexane, toluene, ethanol (EtOH), isopropanol (IPA), acetonitrile (MeCN), and butanol) were purchased from Sigma Aldrich and used as received. Oleylamine (OAm, technical grade, 70%) was purchased from Sigma Aldrich and purified before use by freezing, thawing, and then centrifuging to remove any insoluble solids. The resulting purified oleylamine was dried under dynamic vacuum before use. Formamide (FA, 99.5%) and oleic acid (OA, 90%) were purchased from Sigma Aldrich and dried under dynamic vacuum before storage in a nitrogen glove box. Cesium chloride (ultra dry, 99.998%), lithium chloride (ultra dry, 99.9%), potassium chloride (ultra dry, 99.95%), cesium bromide (ultra dry, 99.9%), lithium bromide (ultra dry, 99.9%), potassium bromide (ultra dry, 99.9%), gallium(iii) iodide (ultra dry, 99.999%), gallium(iii) chloride (ultra dry, 99.999%), potassium iodide (ultra dry, 99.998%), lithium iodide (anhydrous, 99.95%), and N,N-dimethylformamide (DMF, anhydrous 99.9%) were purchased from Alfa Aesar and used as received. Lithium sulfide (98%) and indium(iii) chloride (anhydrous, 99.999%) were purchased from Strem Chemicals and used as received. Lithium selenide was synthesized from lithium triethylborohydride and selenium pellets as described previously. 32,33

InP QDs. 3.8 nm diameter InP QDs were provided by Nanosys, Inc. as a solution in ODE and were stored in a nitrogen glove box. The QDs were precipitated by addition of EtOH and centrifugation and redispersed in toluene for further processing.

(NH₄)₂S Ligand Exchange. A solution of as-synthesized InP QDs dispersed in toluene (4 mL, 5 mg/mL) was layered atop a solution of 50 μ L (NH₄)₂S (40–48 wt % aq.) in 2 mL formamide.³⁴ The mixture was stirred until all QDs were transferred to the formamide phase. The toluene phase was removed, and the formamide phase was washed three times with 5 mL fresh toluene. The (NH₄)₂S-capped QDs were precipitated by adding MeCN and toluene nonsolvents and centrifugation. The QDs were washed once more with formamide/MeCN/toluene, and then the pellet was washed with MeCN/toluene to remove residual formamide. The pellet was allowed to dry overnight under nitrogen at room temperature.

 $L\bar{i}_2S$ Ligand Exchange. A solution of as-synthesized InP QDs dispersed in toluene (4 mL, 5 mg/mL) was layered atop 2 ml of a freshly prepared 0.0125(M) solution of Li_2S in formamide. The mixture was stirred until all QDs were transferred to the formamide phase. The toluene phase was removed, and the formamide phase was washed three times with 5 mL fresh toluene.

(DDA)₂S Ligand Exchange. Following the above procedure, a solution of (NH₄)₂S or Li₂S-capped InP QDs was prepared in formamide (2 mL, 10 mg/mL). A solution of ~400 mg DDAB in 2 mL toluene was added to the formamide solution and mixed well. The QDs were quickly transferred into the toluene phase. The formamide phase was discarded, and the toluene phase was washed with EtOH to remove excess DDAB. The (DDA)₂S-capped InP QDs could be redispersed in toluene or hexane.

Li₂Se Ligand Exchange. A solution of as-synthesized InP QDs dispersed in toluene (10 mL, 2 mg/mL) was layered atop a solution of Li₂Se in formamide (2 mL, 0.1 M). The mixture

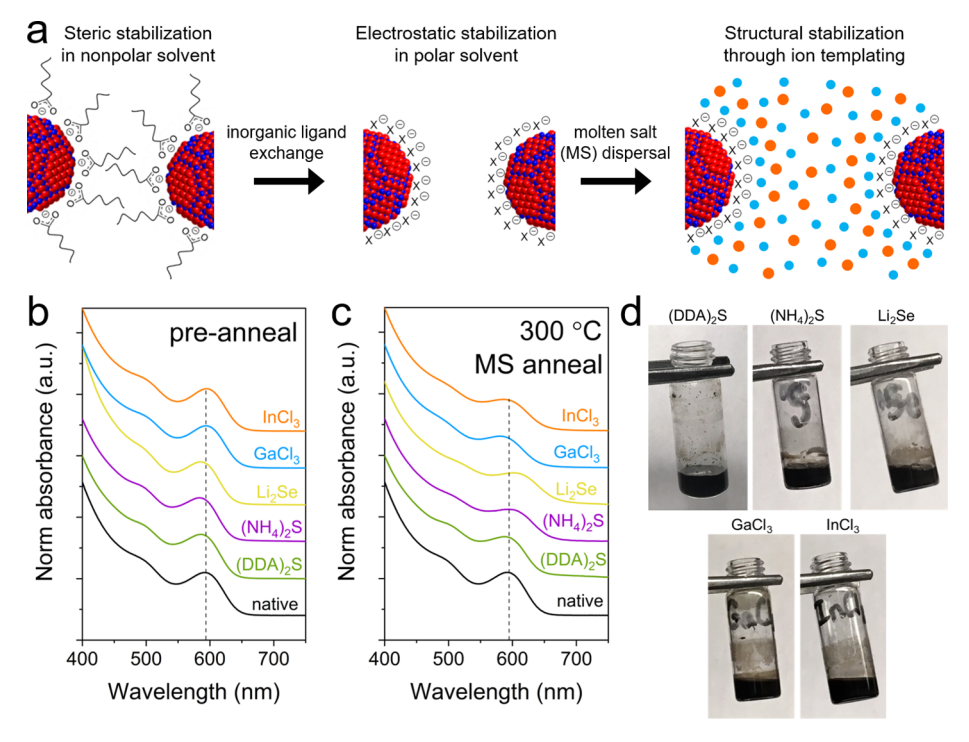


Figure 1. (a) Schematic illustrating the role of surface ligands in the dispersal of QDs in nonpolar solvents, polar solvents, and molten salts. Long-chain organic ligands provide stabilization in nonpolar solvents through steric repulsion, charged inorganic surface ligands provide stabilization in polar solvents through electrostatic repulsion, and chemical interactions between the NC surface and coordinating molten salts provide stabilization through ion correlations (blue: cation and orange: anion). (b) Solution absorbance spectra of InP QDs before molten salt dispersal and annealing show near identical features for particles with different surface chemistries. (c) Solution absorbance spectra for solutions of InP QDs with different initial surface chemistries following molten salt dispersal at 300 °C show slightly broadened and shifted features. (d) Photographs of uniform dispersions of InP QDs in molten bromide eutectic at 300 °C, with different surface chemistries indicated.

was stirred until all QDs were transferred to the formamide phase. The toluene phase was removed, and the formamide phase was washed three times with 10 mL of fresh toluene. The Li₂Se-capped QDs were precipitated with MeCN and centrifugation. The QDs were washed with formamide/MeCN/toluene, and then the pellet was washed with MeCN to remove residual formamide. The pellet was allowed to dry overnight under nitrogen.

GaCl₃ and InCl₃ Ligand Exchanges. The MCl₃ ligand exchanges were adapted from a procedure reported by Dirin et al. A solution of as-synthesized InP in hexane (10 mL, 2 mg/mL) was layered atop a solution of MCl₃ in DMF (2 mL, 0.05 M) and stirred until all particles were transferred to the DMF phase. The particles were precipitated by the addition of toluene and centrifugation and redispersed with DMF plus 10 vol HMPA. This washing procedure was repeated three times. The particles were then redispersed with acetonitrile, washed with a mixture of toluene and hexane, and allowed to dry overnight under nitrogen.

Molten Salt Dispersal. A bromide eutectic mixture was formed by combining CsBr, LiBr, and KBr in the molar ratio 25:56.1:18.9 (melting point 236 °C) and mixed well with a mortar and pestle. A portion of 1.5 g of the bromide eutectic mixture was combined with the ligand exchanged QDs. For the (DDA)₂S passivated particles, the QDs were added to the salt as a solution in toluene and the toluene was removed by evaporation at 140 °C before further heating. A similar protocol was followed while using either an iodide eutectic mixture obtained by combining KI and LiI in the molar ratio 36.9:63.1 (melting point 250 °C) or a chloride eutectic mixture obtained by combining CsCl, KCl, and LiCl in the

molar ratio 29.2:13.3:57.5 (melting point 265 °C) and ground into a fine powder with a mortar and pestle. For the other surface ligands, the NCs were added to the bromide salt as a dry powder and were combined in a mortar and pestle. The salt/QD mixture was loaded into a 4 mL glass vial and heated at 300 °C with vigorous stirring (using a glass-coated stir bar) for 1–3 h to form a homogenous dispersion. We provided the photographs of such (visually) homogeneous particle dispersions in the molten bromide eutectic, Figure 1d. Previously reported SAXS measurements further confirmed the homogeneous dispersion of NCs in the molten salt medium.²⁴

Molten Salt 400 °C Annealing. After dispersal of the QDs in molten bromide eutectic at 300 °C, the mixture was cooled to room temperature and transferred into a muffle furnace. The QD/salt dispersion was heated at 400 °C for 1 h.

Gallium Cation Exchange. After dispersal of the QDs in molten bromide eutectic at 300 $^{\circ}$ C, the mixture was cooled to room temperature and 230 mg of GaI₃ (0.5 mmol) was added to the salt mixture. The mixture was heated at 300 $^{\circ}$ C with vigorous stirring for an additional hour to fully incorporate the gallium salt. After cooling to room temperature, the salt mixture was transferred into a muffle furnace and heated at an elevated temperature (380–430 $^{\circ}$ C) for the desired reaction time (1–16 h). Higher temperatures and longer reaction times led to increased gallium incorporation.

QD Recovery following Molten Salt Treatment. The bromide salt matrix was dissolved in 80 $^{\circ}$ C formamide (\sim 10 mL), and the QDs were recovered as a solid by centrifugation. The QD solid was washed with 4 mL of fresh formamide to remove residual salt. The particles could regain colloidal stability in nonpolar solvents through treatment with either

OA/OAm or $(NH_4)_2S$ and DDAB (S/DDA). To recover the particles with OA/OAm, the QD powder was combined with 2 mL of toluene, 100 μ L of OA, and 100 μ L of oleylamine and stirred at 50 °C for 45 min. The resulting QD solution in toluene was washed with ethanol to remove excess ligands and then stored in toluene or hexane. For S/DDA recovery, the QD powder was dispersed in 2 mL of formamide using either 30 μ L of $(NH_4)_2S$ solution or 250 μ L of a 0.1(M) solution of Li₂S in formamide. A solution of DDAB in toluene was then layered atop the formamide solution, and the QDs were transferred to the toluene phase upon mixing. The QD solution in toluene was washed with ethanol to remove excess ligands, and the particles were redispersed in toluene or hexane.

HF Treatment of $In_{1-x}Ga_xP$ QDs. A solution of 3 mL of hexane, 1 mL of butanol, 2 μ L of 5vol % HF in butanol (2.4 × 10^{-6} mol HF), 50 μ L of $In_{1-x}Ga_xP$ QD solution in hexane (10 mg/mL, \sim 8 × 10^{-9} mol QDs), and \sim 400 mg of TOPO was prepared in a plastic centrifuge tube and sealed under nitrogen in the glove box. In a fume hood, the solution was illuminated by a halogen lamp with a 515 nm long pass filter for 2 h. Absorbance, PL, and PLE spectra of the HF-treated solutions were collected in PMMA cuvettes in air. Note: Higher emission QY was achieved with $10\times$ more concentrated HF treatment, accompanied by an absorbance blue shift and PL broadening.

CHARACTERIZATION

Optical Absorption. UV-vis spectra were collected on colloidal solutions of QDs with a Cary 5000 spectrophotometer.

Emission. PL and PL excitation (PLE) spectra for colloidal solutions of QDs were collected using a Horiba Fluoromax-4 fluorimeter. Unless otherwise stated, PL spectra were acquired with a 430 nm excitation. For both the PL and PLE measurements, the monochromator slits were set at 3 nm at both the entrance and exit slits. The PLE spectra have excitation scatter removed for clarity. QYs were measured by comparison to the reference dye Coumarin-153 (QY 53%).

Powder X-ray Diffraction. Wide-angle powder X-ray diffraction (PXRD) data were acquired on a Bruker D8 diffractometer using a 1.54 Å Cu K- α source and a Vantec 2000 array detector. QD samples were prepared as films on glass or silicon. The $\text{In}_{1-x}\text{Ga}_x\text{P}$ composition was estimated from the position of the [111] peak using Vegard's law. The lattice constant, a, is related to the [111] peak position as follows, where d_{111} is the d-spacing of the [111] plane, λ is the wavelength of the X-ray source, and θ is the peak position

$$d_{111} = \frac{\lambda}{2 \sin \theta}$$
 and $a = d_{111}\sqrt{3}$

Then, the lattice constants of bulk InP (5.8687 Å) and GaP (5.4505 Å) can be used as follows to calculate the alloy composition, x

$$a(In_{1-x}Ga_xP) = (1-x)a_{In} + xa_{Ga}$$

Small-Angle X-ray Scattering. Colloidal solutions of QDs in toluene or hexane were prepared in sealed Kapton capillaries for small-angle X-ray scattering (SAXS) experiments. SAXS patterns were collected using a SAXSLab Ganesha instrument with Cu K α radiation (λ = 1.54 Å). The SAXS curves were analyzed by fitting to a quantitative model in Igor Pro using the Irena package (available at http://usaxs.xray.aps.

anl.gov/staff/ilavsky/irena.html).³⁶ The scattering curves were fit in the particle size distribution module using the model-free maximum entropy approach. Based on TEM data, the particles' form factor was assumed to be that of a sphere with an aspect ratio of 1. The extracted size distributions were further fit with symmetric Gaussians.

Transmission Electron Microscopy. Transmission electron microscopy (TEM) images were obtained on an FEI Technai F30 microscope at 300 kV.

Inductively Coupled Plasma-Optical Emission Spectroscopy. QD samples were prepared for inductively coupled plasma-optical emission spectroscopy (ICP-OES) measurements by thorough washing with ethanol followed by digestion in 0.5 mL of 4:1 HCl (≥37%, TraceSELECT, Fluka): HNO₃ (69.0%, TraceSELECT, Aldrich). The samples were diluted with deionized ultra-filtered water to a concentration of 0.5−25 ppm. ICP-OES analysis was performed using an Agilent 700 Series spectrometer.

X-ray Photoelectron Spectroscopy. X-ray photoelectron spectroscopy (XPS) analysis was performed on a Kratos Axis Nova spectrometer using monochromatic Al $K\alpha$ source (1486.6 eV). In 3d, Ga $2p_{3/2}$, P 2p, and O 1s high-resolution spectra were collected using an analysis area of $0.3 \times 0.7 \text{ mm}^2$ and 20 eV pass energy with the step size of 100 meV. Charge neutralization was performed using a co-axial, low energy ($\approx 0.1 \text{ eV}$) electron flood source to avoid shifts in the recovered binding energy. C 1s peak of adventitious carbon was set at 284.8 eV to compensate for any remaining charge-induced shifts.

RESULTS AND DISCUSSION

Dispersion of InP QDs with Different Surface Ligands in Molten Salts. Solution-processed NCs can be uniformly dispersed in a variety of molten salt media. ^{24,25} To form a stable dispersion, the NC surface chemistry and salt composition must be complementary to allow for chemical interactions at the surface that induce ion templating in the salt matrix. These ion correlations extend beyond the Debye length and prevent close contact of NC surfaces in the salt matrix. ²⁵ To achieve the required surface interaction, as-synthesized NCs capped with long-chain organic ligands must undergo either ligand stripping, creating a bare NC surface, ³⁷ or inorganic ligand exchange, passivating the surface with small inorganic moieties. ^{34,35,38,39} These NCs can then be uniformly dispersed in Lewis basic molten salts, such as alkali halides and thiocyanates (Figure 1a). ²⁴

It has been shown that the dispersal of III-V QDs in a molten salt matrix can allow access to chemical transformations that are impossible in traditional organic media. ^{22,23} Molten salt annealing in the presence of excess Ga3+ improves the GaAs QD lattice structure by healing gallium vacancies²² and induces indium-to-gallium cation exchange in InP and InAs QDs.²³ Previous molten salt studies were conducted primarily on III-V NCs passivated with didodecyldimethylammonium sulfide ((DDA)₂S). It was postulated that at the high temperature of molten salt processing (≥300 °C), the DDA⁺ cations decompose via Hofmann elimination and the salt interfaces with a sulfide-capped QD surface.²³ Here, we seek to understand the role that different surface chemistries can play in the dispersal, phase stabilization, and reactions of III-V QDs in a molten bromide matrix, focusing on InP QDs and indium-to-gallium cation exchange.

To fully understand the role of surface chemistry in the molten salt dispersal and indium-to-gallium cation exchange of InP QDs, we characterized the changes in the QD properties at multiple stages of the synthetic process. Using a consistent batch of 3.8 nm InP QDs (Figure S1; small InP QDs, see Experimental Section), we explored molten salt dispersal at 300 °C and elevated temperature annealing at 400 °C, with or without excess Ga³⁺, for the following surface chemistries: (DDA)₂S, (NH₄)₂S, Li₂Se, GaCl₃, and InCl₃. Sulfide and selenide were chosen due to the previous success with the dispersal of sulfide-capped QDs in molten salts, 22,23,25 the ubiquity of surface chalcogenide treatments for III-V semiconductors, 40 and the established precedent for shelling InP QDs with ZnSe and ZnS. 15,41 Sulfur is known to have relatively high diffusivity in InP at elevated temperatures^{31,42} and could impact the optical and electronic properties of InP and In_{1-x}Ga_xP QDs if it diffuses into the bulk of the QD lattice. 43 To explore similar surface chemistry with a lower probability of diffusion, we studied selenide surface ligands, which should have a lower diffusion coefficient in the InP lattice due to their larger ionic radius.⁴⁴ Additionally, GaCl₃ and InCl₃ surface chemistries were chosen because they will not introduce heterovalent impurities into the system.

The native organic ligands which passivate the assynthesized InP QDs were replaced with small inorganic ligands through two-phase solution ligand exchange following reported procedures. 34,35 In brief, a dilute solution of InP QDs dispersed in a nonpolar solvent (hexane or toluene) is added to an immiscible solution of the desired inorganic ligand in the polar solvent (N,N-dimethylformamide (DMF) or formamide). The inorganic ligands replace the native ligands at the NC surface, and the NC phase is transferred into the polar solvent. Colloidal solutions of (NH₄)₂S and Li₂Se-capped InP QDs in formamide and GaCl₃ and InCl₃-capped InP QDs in DMF have absorbance spectra which are nearly identical to that of the as-synthesized InP QDs, confirming that we have maintained the QD size and monodispersity (Figures 1b and S1). The (NH₄)₂S-capped InP QDs can be transferred back into toluene or hexane using didodecyldimethylammonium bromide (DDAB) as a phase transfer agent to yield (DDA)₂Scapped InP QDs, employing a standard protocol adopted from one of our past publications. 45 Toluene and hexane serve as inert, low boiling point solvents for ease of further processing steps, and the DDA+ should decompose at the high temperatures of molten salt treatment (≥300 °C) to yield a sulfide-capped QD surface.46

The inorganic-capped InP QDs can be well dispersed in a molten bromide eutectic composed of CsBr, LiBr, and KBr in a 25:56.1:18.9 molar ratio (melting point 236 °C). The (NH₄)₂S, Li₂Se, GaCl₃, and InCl₃-capped InP QDs were dried and then combined with the bromide eutectic powder by grinding in a mortar and pestle. In contrast, the (DDA)₂S-capped InP QDs could be added to the bromide salt as a toluene or hexane solution, followed by solvent evaporation to yield a uniform distribution of the QDs throughout the bromide salt powder. The QD/salt mixtures were heated well above the melting point of the bromide eutectic (300 °C) and stirred vigorously for 3 h to achieve uniform dispersions. For all the surface ligands studied, the InP QDs were distributed uniformly throughout the salt matrix (Figure 1d).

To investigate the stability of InP QDs after dispersion in molten salts, we recovered the salt-dispersed QDs as colloidal solutions in a nonpolar solvent. Upon cooling to room

temperature, the QDs are well-dispersed in a solid bromide salt matrix. The bromide salt can be dissolved in formamide, and the QDs are isolated as a powder by centrifugation. The colloidal stability of these QDs can be regained by two different methods. In previous works, the NCs have been recovered through repassivation with (DDA)₂S, as described above. 22,23 To avoid the surface restructuring that takes place upon sulfide exchange, 31,43 here we instead use a combination of OA and OAm (OA/OAm) ligands to recover colloidal stability. The salt-treated QDs regain colloidal stability when stirred in a toluene solution of OA/OAm at 50 °C for 45 min. The resulting QD solution can be washed with EtOH to remove excess organic ligands, and the washed particles retain colloidal stability indefinitely. For each of the QD surface chemistries mentioned above, the QDs were recovered with OA/OAm after molten salt treatment.

Stability of InP QDs during Molten Salt Annealing. Dispersal of the InP QDs in molten bromide eutectic at 300 °C induces minor changes in the QD properties which are largely independent of the initial surface chemistry. After molten salt dispersal and recovery with OA/OAm, the InP QDs initially passivated with (DDA)₂S, (NH₄)₂S, GaCl₃, and InCl₃ can be quantitatively recovered as a colloidal solution in hexane or toluene. The QDs capped with Li₂Se, in contrast, have only limited colloidal stability when recovered with OA/ OAm and must be repassivated with (DDA)₂S to achieve quantitative colloidal stability. We attribute this difference in dispersibility to redox reactions at the surface of the selenidecapped QDs, for instance, oxidation to produce diselenide surface species.⁴⁸ For all surface chemistries studied, there is mild ripening of the InP QDs during molten salt treatment at 300 °C. This increase in particle size distribution broadens the absorbance spectra (Figures 1c and S2), decreasing the prominence of the excitonic features and increasing the halfwidth at half maximum (HWHM) of the first excitonic peak. This peak broadening is qualitatively similar for all of the studied surface chemistries. Additionally, the position of the first excitonic peak slightly shifts after molten salt annealing at 300 °C, with redshifts observed for chalcogenide passivated InP QDs and blue shifts observed for GaCl₃ and InCl₃ passivated QDs. This can be explained either by the changes in average particle size or by the changes in surface chemistry which can impact the positions of the band-edge states.⁴⁹ The observed effects are subtle, rendering it difficult to deconvolute the effects of these two possibilities. For all the studied surface chemistries, the XRD patterns for the InP QDs recovered after molten salt annealing at 300 °C, show peaks nearly identical to the initial QDs with no appreciable change in peak breadth or appearance of impurity phases (Figure S3).

More pronounced changes in the InP QD structure and properties can be observed after molten salt annealing at higher temperatures. Although III–V QDs have been regarded as more robust than many other NC systems due to their resistance to ripening and grain growth at high temperatures, ^{50,51} the InP phase has relatively poor thermal stability due to the high equilibrium vapor pressure of phosphorus above InP at elevated temperatures. ²⁷ The decomposition of bulk InP starts around 500 °C, ⁵² though it can be mediated by saturating the atmosphere with phosphorus or modifying the InP surface. ^{30,53,54} We can expect that the thermal decomposition of InP will occur at even lower temperatures in nanocrystalline materials due to their high surface to volume ratio.

Changes occur in the structure and properties of InP QDs annealed in molten bromide eutectic at 400 °C, which show an interesting dependence on surface chemistry and suggest that surface chemistry may be able to tune the QD reactivity in molten salts. After dispersing the inorganic-capped InP QDs in molten bromide salt at 300 °C, the salt mixture was annealed at 400 °C for 1 h. Then the salt was dissolved and the QD powder was treated with OA/OAm as described above. For each of the surface chemistries tested, only a small amount (<5%) of the InP QDs could be recovered as a colloidal solution in toluene after molten salt annealing at 400 °C. The solution absorbance spectra were measured for the colloidal material (Figure S2), and the residual powders were analyzed by XRD (Figures 2 and S3). The XRD patterns show that the (DDA)₂S and Li₂Se-treated InP QDs remain stable at high temperatures, with major peaks corresponding only to nanocrystalline InP, while the (NH₄)₂S-, GaCl₃-, and InCl₃treated samples have peaks corresponding to both nanocrystalline InP and decomposition products (indium metal and In₂S₃) due to the loss of phosphorus under these conditions

$$4 \operatorname{InP} \rightarrow 4 \operatorname{In}(0) + P_{4} \uparrow$$

$$2 InP + 3 (NH_4)_2 S \rightarrow In_2 S_3 + 2 PH_3 \uparrow +6 NH_3 \uparrow$$

The InP decomposition mechanism is in accordance with the mechanism of bulk InP decomposition as described in prior literature. As we observed the formation of elemental metallic indium as one of the decomposition products (via PXRD, Figure 2); the mechanism as described is the most likely one. The In₂S₃ impurity peaks in the XRD pattern for the (NH₄)₂S-passivated InP QDs after 400 °C annealing (Figure 2c) can also result from the presence of residual polysulfide species ((NH₄)₂S_n, n > 1) in the salt melt, which are known to form in the aqueous (NH₄)₂S solution used for ligand exchange standard and be highly oxidizing

$$2 \text{ InP} + (NH_4)_2 S_n \rightarrow \text{In}_2 S_3 + (NH_4)_2 S_{n-3} + 1/2 P_4 \uparrow$$

The formation of an In_2S_3 phase is not observed for (DDA)₂S-passivated InP because the excess polysulfide is likely removed in further phase transfer and washing steps, while the Li_2 Se-passivated InP QDs are treated with high purity Li_2 Se that does not contain polychalcogenides. As a control experiment, we show that InP QDs passivated with high purity Li_2 S and annealed in molten bromide at 400 °C have no In_2S_3 peaks in the XRD pattern and a smaller contribution from metallic indium (Figure S4). Thus, the decomposition of sulfide passivated InP QDs at elevated temperatures may be controlled by using Li_2 S or more thorough washing of the (NH₄)₂S-passivated particles. We nonetheless show below that the (NH₄)₂S-passivated InP particles largely maintain their particle size upon 400 °C molten bromide annealing.

One can notice slight deviations in the InP X-ray peak positions from the bulk values in Figure 2b,c,e. Small tightly bound surface ligands such as sulfide and gallium chloride etc. may impose compressive lattice strain on the nanoparticles. These small distortions may have led to slightly shifted peak positions in the diffractogram. No shifts are observed for InP QDs capped with larger selenide and indium chloride ligands (Figures 2d,f). The data in Figure S3 further confirm that these X-ray peak shifts are intrinsic to the surface chemistry (i.e. they are observed after the ligand exchange) and not an effect of high temperature annealing.

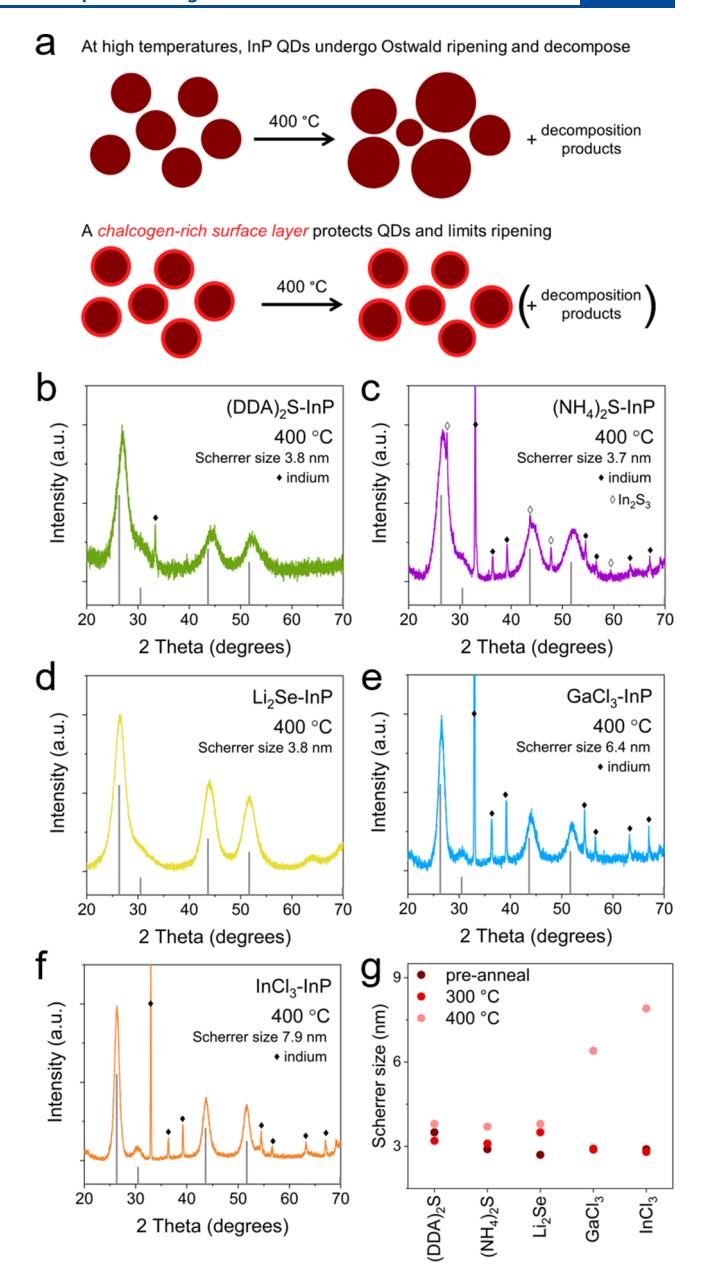


Figure 2. (a) Schematic illustrating how chalcogenide ligands form a protective surface layer on InP QDs, which limits decomposition and grain growth at high temperatures. (b–f) PXRD patterns for InP QDs after heating at 400 °C in molten bromide eutectic with peak positions and intensities for bulk InP given as grey bars. QDs passivated with (b) (DDA)₂S and (d) Li₂Se show little evidence of decomposition and minimal grain growth. QDs passivated with (c) (NH₄)₂S, (e) GaCl₃, and (f) InCl₃ have impurity peaks corresponding to particle decomposition. (g) Scherrer sizes calculated from the XRD patterns for InP QDs following ligand exchange and molten bromide annealing at 300 and 400 °C. QDs passivated with GaCl₃ and InCl₃ show significant grain growth at 400 °C.

The XRD patterns show a difference in the crystallite size for chalcogenide and metal halide-treated InP QDs following 400 °C molten bromide annealing. The InP peaks are much sharper in the patterns for the GaCl₃ and InCl₃-treated QD samples following the high temperature annealing (Figure S3d,e); analysis of the Scherrer size for these materials suggests that they have either sintered or undergone significant Ostwald ripening to form larger InP nanocrystallites, increasing from

 \sim 3 nm to over 6 nm in average crystallite size (Figure 2g). The XRD peaks for the annealed InP QDs passivated with chalcogenide ligands show a small decrease in the peak breadth, corresponding to a slight increase in the Scherrer size of these particles (\sim 3 to \sim 3.8 nm). The absorbance spectra for the colloidal fraction of the 400 °C annealed QDs also show broadening and redshifts indicative of particle ripening (Figure S2). This broadening is most pronounced for the QDs treated with InCl₃ and most subtle for the QDs treated with (DDA)₂S, in agreement with the change in the particle size predicted by XRD. Interestingly, the absorbance spectrum for the 400 °C annealed QDs treated with GaCl3 shows both a broad, red shifted onset indicative of particle ripening and blue shifted excitonic peaks. This suggests the GaCl3-treated particles not only ripened, as seen with the InCl3-treated particles, but also underwent partial gallium cation exchange, leading to an absorbance blue shift (see discussion below). The observed differences in decomposition and particle growth for the chalcogenide and metal halide capped InP QDs indicate that the initial surface chemistry can play a significant role in not only the dispersibility of the QDs in the molten salt matrix but also impact the particle stability at elevated temperatures.

Based on elemental analysis of the particles recovered after the 400 °C molten bromide annealing (Table 1), the particles

Table 1. Elemental Analysis of Recovered InP QDs after Annealing in Molten Bromide Eutectic as Determined by ICP-OES, with Initial Surface Chemistry and Annealing Temperature Indicated

	In mol %	P mol %	S or Se mol %
(DDA) ₂ S, 300 °C	49% In	33% P	18% S
$(DDA)_2S$, 400 °C	46% In	32% P	22% S
$(NH_4)_2S$, 300 °C	47% In	31% P	22% S
$(NH_4)_2S$, 400 °C	48% In	28% P	24% S
Li ₂ Se, 300 °C	45% In	30% P	25% Se
Li ₂ Se, 400 °C	46% In	27% P	27% Se

initially passivated with chalcogenides retain a chalcogen-rich surface through the molten salt processing and recovery. This may indicate the formation of a surface shell of metal chalcogenides ($\rm In_2S_3$ or $\rm In_2Se_3$), which acts as a protective layer and prevents QD ripening and decomposition (Figure 2a). The high temperature stabilization of InP surfaces with (NH₄)₂S by the formation of a thin $\rm In_2S_3$ layer is well-documented for bulk crystals, $^{29-31}$ and we expect that selenide will perform a similar function. Moreover, any physical barrier to phosphorus outgassing has been shown to improve the temperature stability of bulk $\rm InP$, 54 so this stabilization phenomenon can likely be extended to other surface chemistries.

The increased stability of chalcogen-passivated InP QDs under molten bromide annealing at 400 °C shows that QD surface groups can act as surfactants at the QD/salt interface. Here, we use the IUPAC definition of the surfactant to mean: a substance which lowers the surface tension of the medium in which it is dissolved, and/or the interfacial tension with other phases, and, accordingly, is positively adsorbed at the liquid/vapor and/or at other interfaces. ⁵⁶

Impact of Surface Chemistry on Indium-To-Gallium Cation Exchange: QD Composition. The above studies illustrate the role that surface ligands play in the dispersion of InP QDs in a molten bromide eutectic and how these surface

ligands impact the high temperature stability of nanocrystalline InP. We seek to use these observations to inform the design of synthetic transformations of InP QDs in molten salt media, specifically indium-to-gallium cation exchange. Our previous work has shown that $(DDA)_2S$ -passivated InP QDs dispersed in molten salt undergo cation exchange to produce $In_{1-x}Ga_xP$ QDs when heated above 380 °C in the presence of excess Ga^{3+} (Figure 3a).²³ The extent of cation exchange controls both the lattice constant and the band gap of the resulting alloy (Figure 3b).⁵⁷ Thus, by controlling the QD size and alloy composition, the absorbance and emission energies as well as the lattice match with wide band gap shelling materials may be tuned. We seek to understand if changes in the surface chemistry of the initial InP QDs impact the properties of the resulting $In_{1-x}Ga_xP$ alloy QDs.

When GaI3 is added to the molten bromide eutectic, high temperature annealing of the InP QD mixture results in indium-to-gallium cation exchange for all surface chemistries tested. The (DDA)₂S, (NH₄)₂S, Li₂Se, GaCl₃, and InCl₃treated InP QDs were dispersed in molten bromide eutectic at 300 °C as described above. Then, a stoichiometric excess of GaI₃ (~5:1 Ga/In) was added, and the salt mixture was stirred for an additional hour at 300 °C. About 0.5 mmol GaI3 was used for ~20 mg of as-synthesized InP nanoparticles. After thorough incorporation of Ga³⁺ into the salt mixture, the QD dispersion was annealed at 400 °C for 1 h. Using the OA/ OAm recovery method, the QDs initially passivated with (DDA)₂S, (NH₄)₂S, or GaCl₃ could be quantitatively redispersed as a colloidal solution in toluene or hexane which remained stable indefinitely. The QDs were initially passivated with InCl₃, and Li₂Se showed poorer colloidal stability following OA/OAm recovery. PXRD patterns for the products collected after 400 °C annealing in the presence of Ga³⁺ show broad peaks corresponding to a nanocrystalline phase with peak positions between those of the InP and GaP standards, suggesting that an In_{1-x}Ga_xP alloy has formed for all samples (Figure 3c). Successful indium-to-gallium cation exchange can also be observed by the pronounced blue shift in the absorbance onset for each of the surface chemistries studied (Figure 3d).

Though differences in surface chemistry show marked effects on the phase stability of InP QDs when annealed at 400 °C without Ga³⁺, the cation exchange products resulting from different initial surface chemistries are quite similar. PXRD patterns for the Ga³⁺-treated material show negligible peak broadening and no impurity peaks for each of the surface chemistries studied (Figures 3c and S3 and S5a). Moreover, the products were much more successfully recovered as a colloid following cation exchange as compared to the poor recovery (<5%) following the control InP QDs annealed at 400 °C without addition of Ga³⁺. This indicates that the cation exchange conditions impart additional stability to the InP phase and nanocrystalline morphology. In addition, the surface coordination of Ga³⁺ may create stronger interactions between the QD surface and the salt matrix, causing better dispersion of the QDs in the matrix and thus preserving the QD size by preventing direct QD surface contact and sintering.

The QD morphology following cation exchange was examined using TEM and SAXS. TEM images of the InP QDs before cation exchange and a representative $In_{1-x}Ga_xP$ QD sample show that the particles have maintained their approximate size and shape (Figure S6). We can use SAXS of the colloidal QD solutions to more accurately quantify the

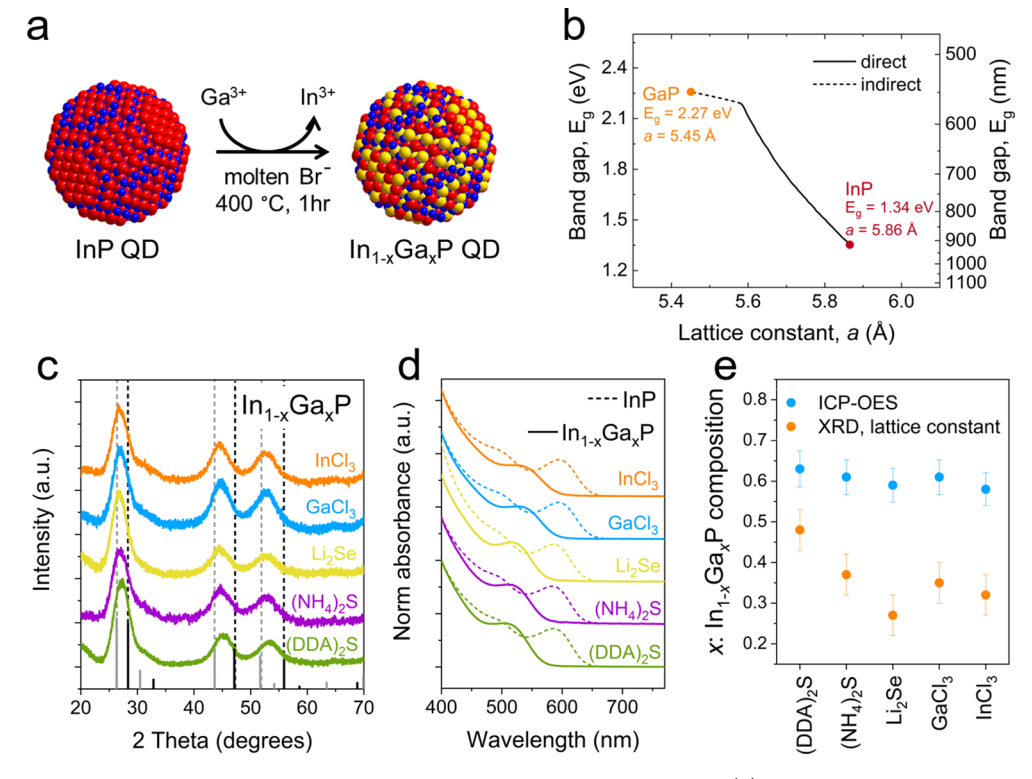


Figure 3. (a) Schematic illustrating indium-to-gallium cation exchange in molten bromide salt. (b) Relationship between the band gap and lattice constant for $In_{1-x}Ga_xP$ alloys, adapted from ref 57. (c) XRD patterns for gallium-exchanged $In_{1-x}Ga_xP$ QDs with different initial surface chemistries. Standard patterns are given for InP (grey) and GaP (black). (d) Solution absorbance spectra for InP and $In_{1-x}Ga_xP$ QDs with different initial surface chemistries show an expected blue shift upon cation exchange. (e) Compositions for $In_{1-x}Ga_xP$ particles with different initial surface chemistries, calculated from elemental analysis (ICP-OES) (blue spheres) and from the lattice constant measured via XRD (orange spheres). The much higher gallium incorporation indicated by elemental analysis that is not reflected in the measured lattice constant suggests the formation of a Ga-rich surface layer.

Table 2. $In_{1-x}Ga_xP$ QD Diameters and Standard Deviations Calculated from Fits to SAXS Patterns and Estimated Composition from XRD and Elemental Analysis of Recovered $In_{1-x}Ga_xP$ QDs after Molten Salt Cation Exchange

	$In_{1-x}Ga_xP$ QD diameter (nm)	calculated x (XRD)	calculated x (ICP-OES)	calculated x (XRF)	In mol % (ICP-OES)	Ga mol % (ICP-OES)	P mol % (ICP- OES)	S or Se mol % (ICP-OES)
$(DDA)_2S$	3.4 ± 0.6	0.48	0.63	0.61	20%	33%	38%	9% S
$(NH_4)_2S$	3.5 ± 0.6	0.37	0.61	0.60	20%	31%	39%	10% S
Li ₂ Se	3.5 ± 0.5	0.27	0.59	0.58	21%	31%	36%	12% Se
$GaCl_3$	3.5 ± 0.7	0.35	0.61	0.53	22%	35%	43%	
$InCl_3$	3.3 ± 0.6	0.32	0.58	0.48	23%	33%	44%	
a	1							

^aInitial surface chemistry of the particles is indicated.

particle size and size distribution before and after cation exchange. Fits of the solution SAXS patterns indicate that the initial InP QDs have a diameter of 3.8 nm with a standard deviation of 0.5 nm (Figure S7), while the $In_{1-x}Ga_xP$ QD diameters decrease to 3.3–3.5 nm with a slight increase in polydispersity (Table 2, Figure S8). Since GaP (a = 5.4505 Å) has a smaller lattice constant than InP (a = 5.8687 Å), we expect the particle volume to decrease due to lattice contraction upon cation exchange. Based on SAXS data, we do not observe a significant difference in $In_{1-x}Ga_xP$ QD size or polydispersity as a function of the initial surface ligand.

The extent of indium-to-gallium cation exchange for each of the surface ligands can be estimated based on the shifts in PXRD, absorbance, and emission peaks as well as elemental analysis. For an alloy QD with the composition $In_{1-x}Ga_xP$, the XRD peak positions shift to higher angles and the absorbance and emission peaks shift to higher energies with increasing gallium content, x (Figure 3b). We can estimate the

composition of an In_{1-x}Ga_xP sample using Vegard's law, where the change in lattice constant as a function of changing composition is assumed to be linear (see Experimental Section). A recent computational study confirmed that Vegard's law holds well for sub-10 nm size In_{1-x}Ga_xP QDs with a random distribution of Ga and In ions. 59 Based on the measured lattice constant, the composition of the In_{1-x}Ga_xP QDs varies significantly with changes in the initial surface ligand, x = 0.27 - 0.48 (Figures 3c,e). In contrast, the elemental analysis obtained using ICP-OES and X-ray fluorescence (XRF) suggests both a closer similarity in composition for In_{1-x}Ga_xP samples with different surface ligands and also a higher extent of cation exchange, x = 0.58 - 0.63 (Figure 3e and Table 2). Moreover, the differences in the absorbance onset energy as a function of surface chemistry do not correlate to the changes in composition as measured by XRD (Figures 3d and 4a; see further discussion below). Therefore, we suggest that under our experimental conditions, the In_{1-x}Ga_xP QD

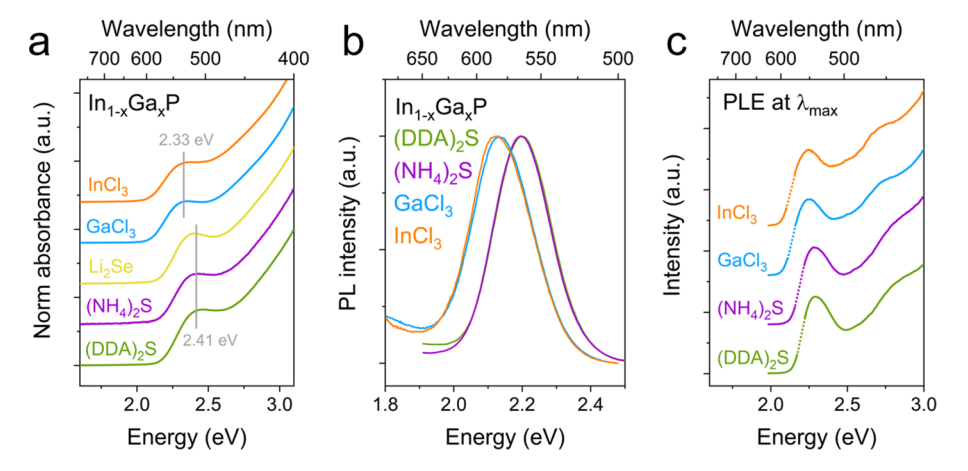


Figure 4. (a) Solution absorbance spectra for $In_{1-x}Ga_xP$ QDs show a difference in the first exciton position with changes in initial surface chemistry. QDs initially passivated by chalcogenides show a more pronounced blue shift upon cation exchange. (b) A similar difference in the peak position based on initial surface chemistry is seen in the PL spectra of $In_{1-x}Ga_xP$ QDs treated with mild HF. (c) PLE spectra monitored at the emission maximum for $In_{1-x}Ga_xP$ QDs with different initial surface chemistry show sharp features.

composition is more accurately predicted by elemental analysis than XRD. ICP-OES elemental analysis of the elements phosphorous and sulfur is often unreliable. Before analysis, the crystals are digested in acids, which could lead to the formation of gaseous products from P and S, as well as a precipitation of elemental sulfur. These can therefore escape and not be measured, leading to underestimating their compositions. The total cation (In + Ga) to anion (P + S) ratios recorded on Table 2 via ICP-OES elemental analysis are within a reasonable range and in agreement with previously reported data. Based on elemental analysis, there are only slight differences in the gallium incorporation for $In_{1-x}Ga_xP$ QDs with different surface chemistries. The differences in alloy composition can be attributed to small variations in experimental conditions (e.g., heating and cooling rates) and do not clearly indicate systematic differences in the extent of cation exchange with different surface ligands.

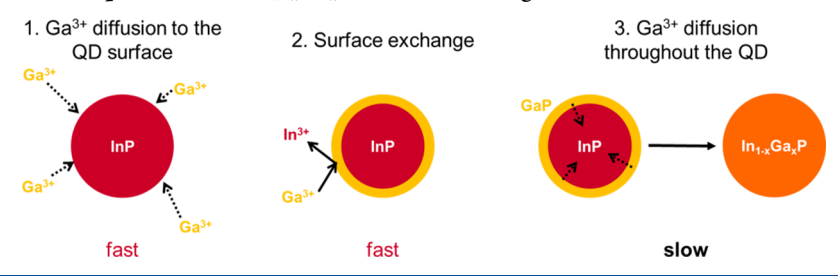
The discrepancies between the In_{1-x}Ga_xP QD alloy compositions estimated by XRD and those measured by elemental analysis can be explained by the impact of surface chemistry on the nanocrystalline lattice and the effects of heterogeneous cation exchange. Changes in the surface coordination of small NCs can induce lattice strain,61-63 which impacts the position and broadening of XRD peaks. Here, we observe small changes in the XRD peak positions of ligand exchanged InP QDs before molten salt dispersal due to differences in the QD surface chemistry (Table S1). Thus, the measured XRD peak positions of the In_{1-x}Ga_xP QDs are a convolution of surface chemistry and lattice composition, which may cause a wide variation in composition predicted by XRD in contrast to the narrow range of compositions measured by elemental analysis. The much higher gallium incorporation indicated by elemental analysis that is not reflected in the measured lattice constant suggests the formation of a Ga-rich surface layer. The 3.8 nm diameter QDs used in this study have approximately 30% of their atoms at the surface. Thus, one can imagine that changes in the composition of the outer surface layer can dramatically change the QD composition with only a minor impact on the QD interior. For example, if a monolayer of metal-rich InP exchanges to GaP, the elemental composition could be up to 30% gallium, while the XRD pattern would show only minor changes resulting primarily from the surface strain rather than

bulk lattice reorganization. Previous studies of ion exchange in semiconductors suggest that ion exchange at the surface occurs quickly while diffusion limits the rate of ion exchange in the bulk.²⁸ Self-diffusion of metal ions in InP and GaP is known to be very slow at the temperature of our cation exchange reaction, 42,64 and though we can expect faster diffusion in a nanocrystalline material, 65,66 we still expect that diffusion into the bulk is the slowest step in indium-to-gallium cation exchange. Therefore, the discrepancy in the In_{1-x}Ga_xP compositions determined by elemental analysis and XRD indicates that under our reaction conditions, we have not formed an equilibrium solid solution but have rather formed a kinetically trapped heterogeneous alloy. Given that In_{1-x}Ga_xP forms a solid solution in all compositions, 67 we expect that experimental conditions can be modified to achieve homogenous In_{1-x}Ga_xP QDs.

Impact of Surface Chemistry on Indium-To-Gallium Cation Exchange: Optical Properties. In addition to the influence of surface chemistry on the phase stability and extent of cation exchange, we sought to understand its impact on the optical properties of the resulting $In_{1-x}Ga_xP$ QDs. The absorbance spectra for the $In_{1-x}Ga_xP$ QDs with different surface chemistries look broadly similar. Each cation exchanged sample shows a significant blue shift of the absorbance onset due to the increased band gap of the alloy and a decrease in the excitonic peak prominence (Figures 3d and 4a). The poor resolution of the excitonic features can be partially attributed to an increase in particle polydispersity. Additional broadening likely results from the heterogeneity of the $In_{1-x}Ga_xP$ alloy composition across individual particles of the ensemble.

The PL spectra for $In_{1-x}Ga_xP$ QDs also show a pronounced blue shift upon cation exchange, confirming the increased band gap with gallium incorporation (Figures S1 and S9). After recovery with OA/OAm, the $In_{1-x}Ga_xP$ QDs have weak PL (<1% QY) with a band-edge peak at 560–580 nm and a very broad red peak, which can be attributed to surface trap emission (Figure S9).⁶⁸ The PL efficiency is higher for $In_{1-x}Ga_xP$ QDs recovered with (DDA)₂S; however, we sought to avoid surface restructuring by (NH₄)₂S_n in our recovery process.^{31,43} Instead, we increased the QY of the OA/OAm recovered $In_{1-x}Ga_xP$ QDs using air-free treatment with dilute HF and visible light (Figure S10). Treatment of InP QDs with

Scheme 1. Illustration of the Steps of InP to In_{1-x}Ga_xP Cation Exchange



dilute HF accompanied by light or heat is a well-established practice for improving the PL QY through surface trap passivation. 17,49,68,69 We chose conditions for HF treatment that increased the PL efficiency (up to ~5% QY) without significantly broadening or shifting the absorbance or emission features of the $In_{1-x}Ga_xP$ QDs (Figure S11 and S12, see Experimental Section). Harsher treatment with more concentrated HF and/or oxygen exposure increased the QY further (up to 20% QY) but was accompanied by broadening and blue shifting of the absorbance and emission features, which have previously been attributed to QD oxidation and etching (Figure S13). 17,69 Notably, the PL for Li_2 Se-passivated $In_{1-x}Ga_xP$ QDs was not improved by treatment with HF or (DDA)₂S. We attribute the poor PL efficiency of Li_2 Se-passivated $In_{1-x}Ga_xP$ QDs to persistent surface traps, which are well known for selenide-rich QD surfaces. 70,71

After cation exchange and dilute HF treatment, the PL spectra for In_{1-x}Ga_xP QDs are 40-60 meV broader than that of the initial InP QDs (Figures S1 and S11). The PL FWHM for the as-synthesized InP QDs is 155 meV and increases to 195 meV for the chalcogenide-passivated In_{1-x}Ga_xP QDs and 215 meV for the metal halide-passivated In_{1-x}Ga_xP QDs. We attribute the PL broadening to a combination of increased QD polydispersity and inhomogeneity of In_{1-x}Ga_xP composition across individual QDs in the ensemble. Using PLE spectroscopy, we can probe the absorbance of a homogenous subset of In_{1-r}Ga_rP QD emitters. For each of the ligand chemistries studied, PLE spectra reveal that narrow emission bands correspond to discrete In_{1-x}Ga_xP QD populations with welldefined excitonic features in their absorbance spectra (Figures 4c and S12). We, therefore, expect that narrow ensemble emission spectra can be achieved for In_{1-x}Ga_xP QDs by optimizing the synthetic conditions to achieve improved control over the particle polydispersity and the homogeneity of cation exchange.

Following molten salt cation exchange, the chalcogenide and metal halide-treated QDs show a systematic difference in their band gaps which cannot be explained by the gallium content or particle size. The absorbance and emission peaks for the $(DDA)_2S$, $(NH_4)_2S$, and Li_2Se -treated $In_{1-x}Ga_xP$ QDs are shifted 70-80 meV higher in energy than the peaks for GaCl₃ and InCl₃-treated In_{1-r}Ga_rP QDs (Figures 4a,b and S9). This blue shift could be rationalized by either the smaller size of the chalcogenide-treated In_{1-x}Ga_xP QDs, which would increase the quantum confinement, or by more complete gallium incorporation for the chalcogenide-treated In_{1-x}Ga_xP QDs, which would increase the band gap. However, fits to the SAXS curves for the colloidal In_{1-x}Ga_xP QDs show that the chalcogenide-treated particles are equivalent in diameter to the metal halide-treated particles (Table 2 and Figure S8), and elemental analysis does not indicate a systematic difference in the extent of gallium incorporation for chalcogenide and metal

halide-treated In_{1-x}Ga_xP QDs (Figure 3e and Table 2). We suggest that the observed difference in band gap for the chalcogenide and metal halide-treated particles can be attributed to the formation of a higher bandgap chalcogenide-rich shell of (Ga/In)₂S₃ or (Ga/In)₂Se₃ on the surface of the alloyed $In_{1-x}Ga_xP$ particles. The surface coordination could impact the confining potential and consequently affect the band energies of the In_{1-r}Ga_rP particles without distorting the size distribution as measured by SAXS. Elemental analysis confirms that the chalcogenide-treated In_{1-x}Ga_xP QDs retain ~10 mol % chalcogen throughout the molten salt cation exchange process (Table 2). Previous studies on InP QDs showed that surface groups can impact the emission wavelength and charge carrier lifetimes of these emitters. 72,73 Further photophysical studies will be needed to thoroughly understand the role of surface chemistry in the recombination mechanism for In_{1-x}Ga_xP QDs.

Discussion of the Cation Exchange Mechanism. To design optimal synthetic conditions for this molten salt cation exchange, we must first develop a more thorough understanding of the reaction mechanism. The indium-to-gallium cation exchange proceeds through three distinct steps shown in Scheme 1. Step 1 is the diffusion of Ga³⁺ from the salt matrix to the InP QD surface. Here, we control this step by flooding the reaction with an excess of Ga³⁺ (~5:1 Ga/In molar ratio) to ensure that the QD is surrounded by a high concentration of Ga³⁺. Step 2 is the surface exchange of In³⁺ to Ga³⁺, which is governed by the thermodynamics of the following reaction^{28,74}

$$InP + Ga(Br, I)_3 \rightleftharpoons GaP + In(Br, I)_3$$

For the indium-to-gallium cation exchange, the reaction favors the creation of a GaP phase due to the higher thermodynamic stability of GaP⁷⁵ and the more favorable solvation of In³⁺ than Ga³⁺ by the soft (according to Pearson's HSAB principle) anions in the salt melt. Step 3 is the diffusion of Ga³⁺ into the lattice and the corresponding out-diffusion of In³⁺. The self-diffusion of In³⁺ in InP and Ga³⁺ in GaP is likely very slow at 400 °C; though we could not find reliable diffusion data in this temperature range, extrapolation from high temperature data suggests diffusion coefficients on the order of 10⁻⁸ nm²/h⁶⁴ and 10⁻¹⁴ nm²/h⁴² for InP and GaP, respectively. Diffusion should be greatly accelerated in nanocrystalline materials due to their high surface to volume ratio and the possibility of lattice deformation around diffusing species. Nonetheless, we expect that the cation diffusion throughout the QD is the rate-limiting step of the cation exchange.

In our previous work on the molten salt cation exchange of III–V QDs, we controlled the extent of cation exchange by modulation of the reaction temperature. For each synthesis, a set amount of InP QDs and GaI₃ was dispersed in a molten bromide eutectic and heated at elevated temperatures (380–

425 °C) for 1 h. Higher temperatures led to more complete cation exchange as evidenced by a more pronounced blue shift in the absorbance and emission spectra and a decrease in the lattice constant. The highest gallium incorporation (In_{0.22}Ga_{0.78}P) was achieved at 425 °C; however, these reaction conditions also led to partial QD decomposition and the In_{1-x}Ga_xP QD yield was not quantitative. Here, we seek to understand if under our reaction conditions, the cation exchange reaction is thermodynamically controlled, where the reaction temperature dictates an equilibrium In_{1-x}Ga_xP composition, or kinetically controlled, where the reaction temperature controls the cation diffusion rate, and the resulting composition is a result of both reaction temperature and reaction time. Understanding and controlling these conditions may allow us to extend our repertoire of cation exchange products, for example, to higher gallium incorporation or controlled heterostructures, while avoiding QD decomposition.

The dual roles of time and temperature in the indium-togallium cation exchange were explored by conducting cation exchange on a consistent set of InP QDs (3.8 nm InP, see Experimental Section) at two temperatures for a series of time points. The as-synthesized InP QDs were ligand-exchanged to (DDA)₂S and dispersed in molten bromide eutectic as described above. This surface chemistry was chosen for its ease of processing. A 5-fold molar excess of GaI3 was added to the salt mixture, and cation exchange was conducted at a given temperature (380 or 400 $^{\circ}\text{C})$ for a set amount of time (1, 4, or 16 h). Following cation exchange, the molten salt matrix was dissolved in warm formamide, and the QDs were redispersed as a colloidal solution in hexane or toluene with (DDA)₂S. For the reactions conducted at 380 °C, the products were quantitatively recovered as a colloidal solution in a nonpolar solvent. However, the harsher reaction conditions at 400 °C led to some QD decomposition and formation of a noncolloidal product, which was negligible after 1 h of reaction but whose formation increased with increasing reaction time.

Under these reaction conditions, the extent of indium-togallium cation exchange increases as a function of both reaction temperature and time. The absorbance and emission spectra for In_{1-x}Ga_xP QDs show an increasing blue shift with longer reaction times (Figures 5a-d and S14 and S15). The blue shift with increasing time is more pronounced for the products obtained at higher temperatures, suggesting that the cation exchange reaction is accelerated at elevated temperatures. This blue shift is accompanied by successive broadening of the absorbance features, though the PL peak remains narrow for all of the $In_{1-x}Ga_xP$ QD samples (48–50 nm FWHM). The PLE spectra monitored at the PL maximum for each of the In_{1-x}Ga_xP QD samples show sharp excitonic features (Figures S14d and S15d). This indicates that the absorbance of individual emitters has not broadened significantly, and the ensemble absorbance broadening observed for the In_{1-x}Ga_xP QDs is related to size or shape polydispersity of In_{1-x}Ga_xP QDs in the ensemble.

The observed blue shift with an increasing reaction time could be attributed either to an increased band gap due to a higher extent of indium-to-gallium cation exchange or to increased quantum confinement due to QD etching in the molten bromide matrix. To quantify the change in QD size, we measured SAXS curves for solutions of the recovered $In_{1-x}Ga_xP$ QDs. Fits to these SAXS curves reveal that the size and size distribution of the $In_{1-x}Ga_xP$ QDs are equivalent for each of the samples after cation exchange under different

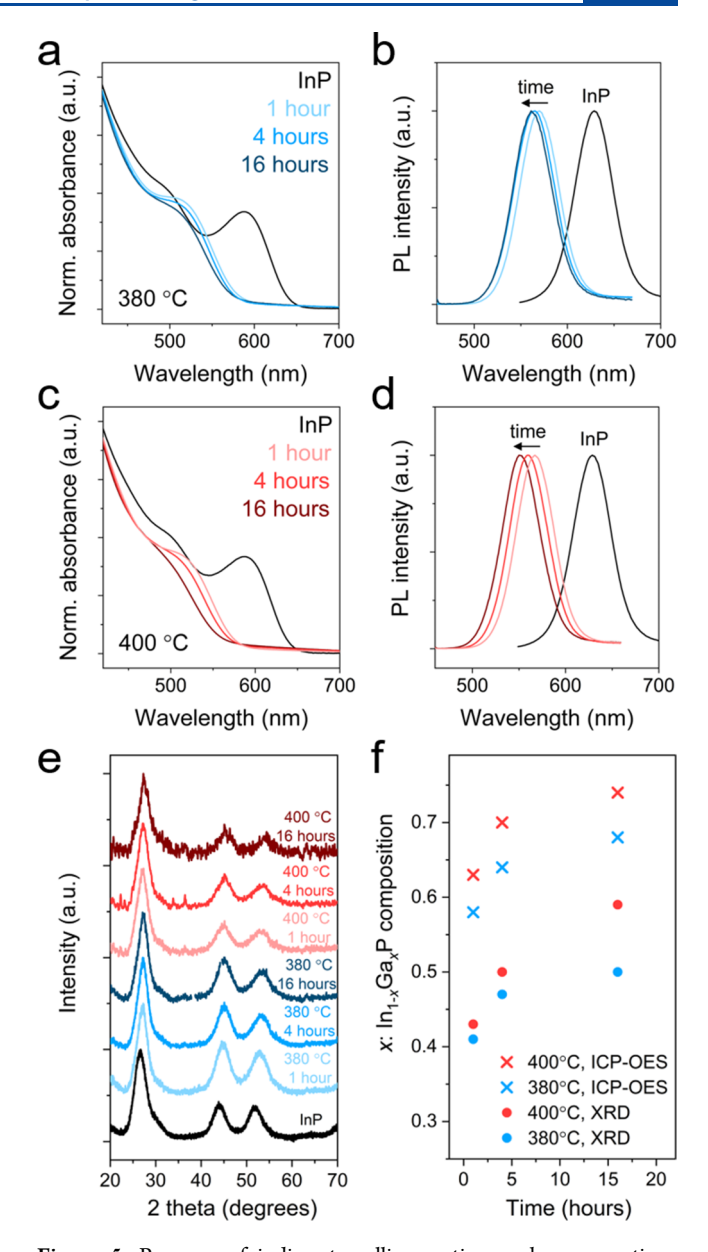


Figure 5. Progress of indium-to-gallium cation exchange reactions depends on both time and temperature. (a,c) Absorbance and (b,d) PL spectra for cation exchange reactions conducted at (a,b) 380 °C and (c,d) 400 °C exhibit increasing blue shifts with increasing reaction time and temperature, indicating increased gallium incorporation. (e,f) This increased gallium incorporation is reflected by the shift in XRD peaks to higher angles and an increase in Ga/In by elemental analysis (ICP-OES).

reaction conditions (Table 3 and Figures S16 and S17), confirming that the observed blue shift correlates to increased gallium exchange. The ${\rm In_{1-x}Ga_xP}$ QDs obtained using the harshest reaction conditions (400 °C, 16 h) show a slight decrease in the size and broadening of the size distribution; these results in concert with the observed non-colloidal product obtained in this synthesis suggest that the QD phase becomes unstable under extreme conditions.

The extent of cation exchange following molten salt annealing at 380 °C and 400 °C was quantified with both PXRD and elemental analysis. The XRD patterns for each of the ${\rm In}_{1-x}{\rm Ga}_x{\rm P}$ samples show broad peaks indicative of a nanocrystalline zinc blende phase which shift to higher angles

Table 3. In_{1-x}Ga_xP QD Diameters and Standard Deviations Calculated from Fits to SAXS Patterns^a

	$In_{1-x}Ga_xP$ QD diameter (nm)
380 °C, 1 h	3.2 ± 0.5
380 °C, 4 h	3.3 ± 0.5
380 °C, 16 h	3.2 ± 0.5
400 °C, 1 h	3.2 ± 0.5
400 °C, 4 h	3.2 ± 0.5
400 °C, 16 h	3.1 ± 0.6

^aThe temperature and reaction time for the cation exchange are noted.

with increasing reaction time (Figure 5e). As described above, we use Vegard's law to estimate the $In_{1-x}Ga_xP$ QD composition based on the XRD peak positions. In accord with the observed optical blue shift, the $In_{1-x}Ga_xP$ QD composition becomes more gallium-rich with increasing reaction time and temperature (Figure 5e,f). Elemental analysis by ICP-OES shows a similar trend in increasing gallium incorporation with time and temperature; however, elemental analysis suggests a higher extent of cation exchange than that estimated from XRD. As discussed above, we ascribe this discrepancy between the lattice constant and the elemental composition to the formation of a gallium-rich QD surface.

The trends in gallium incorporation as a function of both time and temperature provide insight into the indium-togallium cation exchange reaction. At both 380 °C and 400 °C, the gallium content dramatically increases at the 1 and 4 h time points and then increases at a lower rate for the 16 h time point (Figure 5f). These results suggest that the indium-togallium cation exchange is under kinetic control at early times, and the gallium content of the recovered In_{1-x}Ga_xP QDs is limited by ion diffusion throughout the lattice. The seeming composition plateau reached at later times suggests that an equilibrium composition can be achieved for long cation exchange reactions. The more complete cation exchange observed for the higher temperature reactions at each time point indicates both faster cation exchange and an equilibrium composition with more complete gallium exchange at higher temperatures. These findings show that by controlling the indium-to-gallium cation exchange temperature, we can tune the equilibrium composition and by modifying the reaction time, we can control the reaction progress toward this equilibrium composition. These results should prove valuable in designing reaction conditions to yield higher gallium incorporation without decomposition, precise tuning of alloy composition, and controlled formation of heterogeneous alloy QDs with a graded composition.

Effect of Molten Salt Composition on the Indium-to-Gallium Cation Exchange. By exploring other molten salt media under carefully controlled conditions, we achieved $In_{1-x}Ga_xP$ QDs with improved optical properties. The choice of a molten salt reaction medium may impact the properties of $In_{1-x}Ga_xP$ QDs, such as the In-to-Ga ratio, elements distribution, and polydispersity. Additionally, since III–V nanostructures are particularly susceptible to oxidation, it is important to maintain a rigorously oxygen- and moisture-free environment during the cation-exchange process. 13,14,26 To completely eliminate oxygen and/or moisture during NC handling in the evaluation of different salt media, we used anhydrous Li_2S in dry formamide as the source of sulfide ligands for $(DDA)_2S$ passivation before and after the annealing

step, as described in the Experimental Section. The cation exchange reactions were performed in three eutectic halide molten salts: a chloride mixture (CsCl, KCl, and LiCl in the molar ratio 29.2 : 13.3: 57.5; melting point $T_{\rm m}=265~{\rm ^{\circ}C}$); a bromide mixture (CsBr, LiBr, and KBr in the molar ratio 25:56.1:18.9 with $T_{\rm m}=236~{\rm ^{\circ}C}$), and an iodide mixture (KI and LiI in the molar ratio 36.9 : 63.1 with $T_{\rm m}=250~{\rm ^{\circ}C}$). ⁴⁷ In all three cases, we used GaI₃ as the source of Ga(III) because, as shown below, iodide ions have a high affinity to the NC surface and likely serve as surface ligands, thus maintaining a similar NC surface structure in all three media.

The differences in the interaction between the halide salt media and InP QDs can be qualitatively demonstrated in the following simple experiment: 200 mg of the chloride, bromide, and iodide eutectics was loaded into three glass vials, and 2 mL of a 0.2 mg/mL solution of (DDA)₂S passivated colloidal InP QDs in toluene was layered atop the salt mixture in each vial, thoroughly mixed, and allowed to settle. Next, the vials were heated at 60 °C on a hot plate for 2 h, vortexed, and allowed to settle. As seen from the photographs in Figure 6a, the iodide salt has the highest affinity toward the InP particles, allowing it to extract the particles directly from the toluene solution. The hard and soft acids and bases (HSAB) classification can be invoked to rationalize this trend. The In-rich InP QD surface behaves as a soft Lewis acid³⁵ and thus displays higher affinity toward the softer Lewis bases such as iodide ions. We hypothesize that the higher affinity of iodide ions to the QD surface facilitates a more homogeneous dispersion of the InP QDs in an iodide salt matrix as compared to the other halide eutectics studied, leading to a more uniform cation exchange across the QD ensemble.

The cation exchange reactions were performed on InP QDs dispersed in the chloride, bromide, and iodide eutectics at 400 °C for different durations of time between 1 and 16 h. A direct comparison of the absorbance spectra of $In_{1-x}Ga_xP$ QDs recovered (using OA/OAm) after a 1 h reaction shows differences in the sharpness of the excitonic transitions of the $In_{1-x}Ga_xP$ QDs, with the sharpest first excitonic peak observed for the reaction performed in the iodide medium and the broadest spectra for the reactions performed in the chloride molten salt (Figure 6b).

Next, we performed an in-depth comparison of the two best performing systems—bromide and iodide eutectics, utilizing the $(\mathrm{DDA})_2\mathrm{S}$ recovery route. As shown in Figure 6c,e, the UV—vis absorbance spectra exhibit a continuous blue shift of the excitonic feature, indicative of a larger gallium composition as a result of longer annealing. The $(\mathrm{DDA})_2\mathrm{S}$ -passivated $\mathrm{In}_{1-x}\mathrm{Ga}_x\mathrm{P}$ QDs prepared in the iodide salt matrix showed consistently narrower emission spectra compared to similar samples synthesized in the bromide eutectic under otherwise identical reaction conditions (Figure 6d,e). The smallest PL FWHM of 41 nm (~0.16 eV) was achieved for the 4 and 16 h $\mathrm{In}_{1-x}\mathrm{Ga}_x\mathrm{P}$ QD samples synthesized in the iodide eutectic.

We analyzed SAXS patterns of the QD solutions from Figure 6c-f (Figure S18) and found that the extracted parameters quantifying the population distributions are very similar to those in Table 3. There was no systematic difference in the size distributions of $In_{1-x}Ga_xP$ QDs synthesized in the bromide and iodide eutectics, ruling out the effect of size polydispersity as the dominant contributor to the observed difference in PL ensemble linewidths. The observed differences in the optical spectra may be ascribed to a non-uniform distribution of Ga among different $In_{1-x}Ga_xP$ QDs or to different Ga-to-In

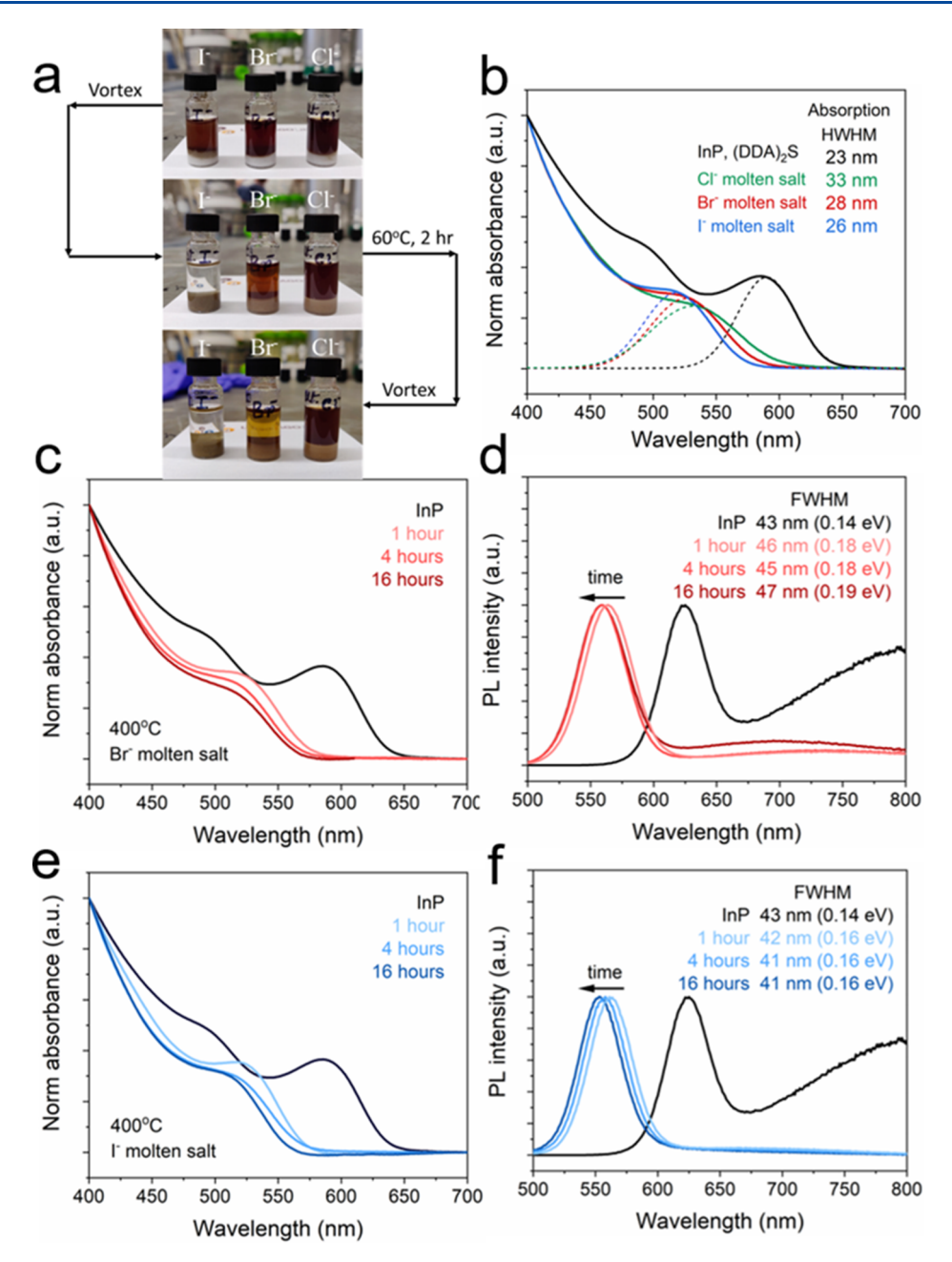


Figure 6. (a) Photographs showing that the affinity of the eutectic salt mixtures toward the $(DDA)_2S$ passivated InP NCs changes in the order $I^- > Br^- > Cl^-$. (b) Comparison of the absorbance spectra of $In_{1-x}Ga_xP$ QD samples synthesized in the chloride, bromide, and iodide eutectic molten salt reaction media utilizing the OA/OAm recovery route. The excitonic features were fitted to a Gaussian to yield the HWHM values quantifying broadening. (c,e) Absorbance and (d,f) PL spectra characterizing the $In_{1-x}Ga_xP$ QD samples synthesized under rigorously oxygen- and moisture-free conditions in the (c,d) bromide and (e,f) iodide eutectic molten salt reaction media following the $(DDA)_2S$ recovery route. The corresponding emission spectra consistently exhibit narrower emission linewidth for cation exchange reactions in the iodide eutectic as compared to the bromide eutectic.

distribution within the QDs reacted in the bromide versus iodide eutectics. Notably, we observe no evidence of particles ripening or sintering upon long-term annealing of the III-V NCs in molten salts.

The PXRD patterns of colloidal $In_{1-x}Ga_xP$ QDs synthesized in different salt matrices each showed peaks corresponding to a nanocrystalline zinc blende phase (Figure S19). The comparison of the extent of gallium incorporation estimated from X-ray diffraction data using Vegard's law, and the elemental analysis data measured by ICP-OES revealed a striking difference between $In_{1-x}Ga_xP$ QDs synthesized in the

bromide (Figure 5f) versus iodide eutectics (Figure 7a). In the bromide medium, the elemental analysis consistently shows an excess of Ga compared to XRD data, which was interpreted as evidence for the formation of a Ga-rich shell and Ga-poor interior. For $In_{1-x}Ga_xP$ QDs prepared in the iodide eutectic, the difference between the estimated compositions measured by the two methods is systematically smaller compared to the bromide case. Remarkably, this disagreement between elemental analysis and the measured lattice constant decreased with time, disappearing in the samples annealed at 400 °C for 16 h. We interpret this observation as evidence for more

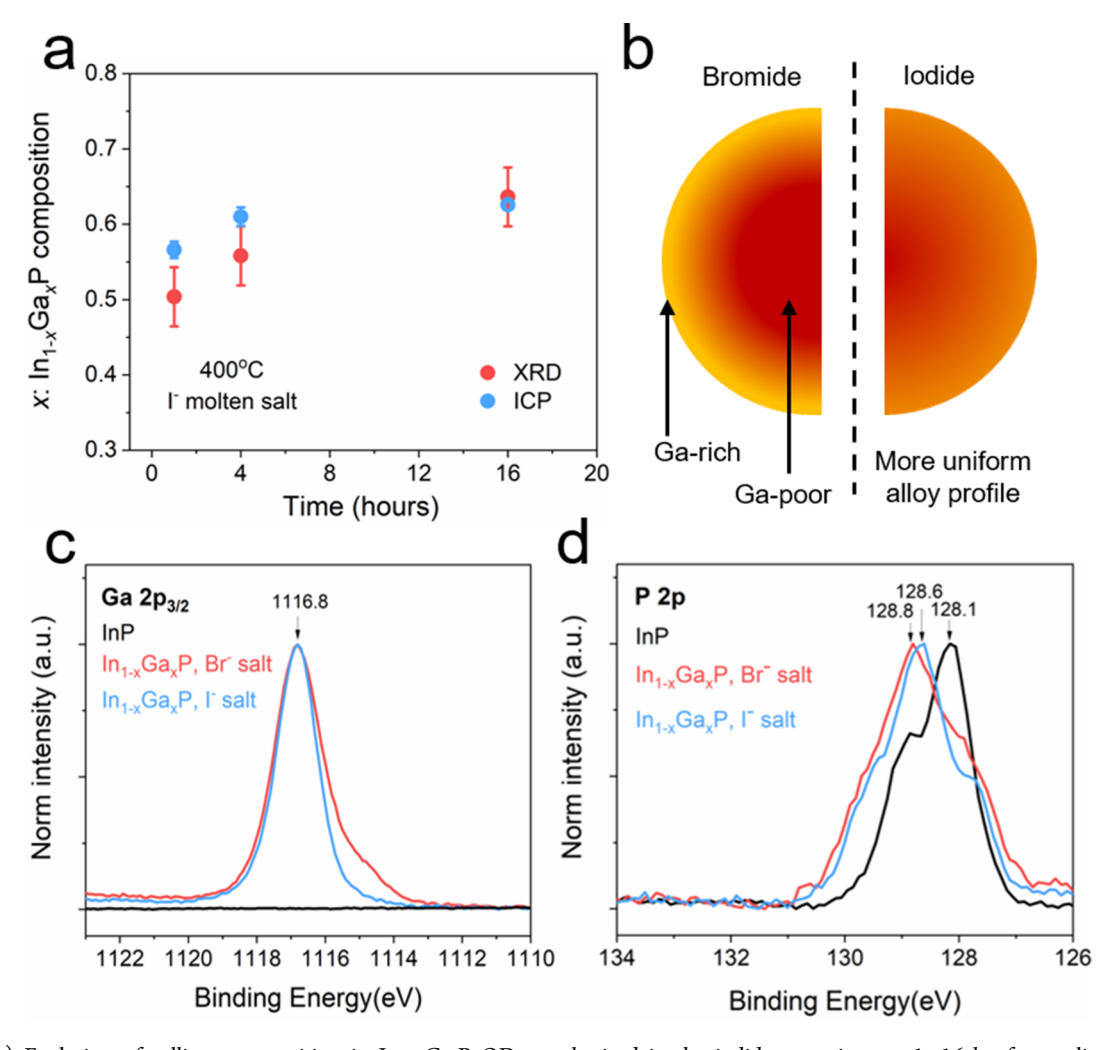


Figure 7. (a) Evolution of gallium composition in $In_{1-x}Ga_xP$ QDs synthesized in the iodide eutectic over 1–16 h of annealing duration, as measured through XRD and ICP-OES elemental analysis. (b) A schematic indicating a more uniform gallium distribution achieved through the iodide synthesis, compared to the bromide synthesis. High-resolution XPS spectra of (c) the Ga $2p_{3/2}$ core level and (d) the P 2p core level of $In_{1-x}Ga_xP$ QDs synthesized in the bromide and iodide eutectics. The XPS peaks are narrower for the iodide synthesis, indicating the presence of a more uniform local coordination environment for both elements.

uniform distribution of Ga within individual $In_{1-x}Ga_xP$ QDs when synthesized in an iodide medium, as schematically shown in Figure 7b. The small size of the $In_{1-x}Ga_xP$ QDs makes it difficult to estimate the elemental distribution within individual QDs by electron microscopy (Figure S20).

Since we used GaI₃ as the Ga(III) source in both cases, the difference in the molten salt compositions likely results in different solvation energies for Ga(III) and In(III) ions, without significantly perturbing other reaction parameters. We propose that the softer iodide salt is a more stabilizing solvent for In³⁺ ions and can help generate a higher equilibrium concentration of In-vacancies at an early stage of the cation exchange reaction. These vacancies are expected to promote the diffusion of Ga(III) deep into the InP QDs rather than forming a thin Ga-rich shell.

XPS measurements of $In_{1-x}Ga_xP$ QDs provide an additional insight into the differences between QDs synthesized in bromide and iodide salts. XPS studies were carried out on the initial InP QDs and $In_{1-x}Ga_xP$ QDs obtained after a 1 h cation exchange reaction in either bromide or iodide eutectic. The peaks observed in the survey spectra are assigned to the photoelectron and Auger lines from expected elements in the

material (Figure S21a-c). High-resolution XPS spectra recorded for the In 3d and Ga 2p3/2 regions indicate the presence of In(III) and Ga(III) species exclusively and no evidence of reduced metallic species (Figures S21d and 7c). Figure 7c compares the Ga $2p_{3/2}$ core levels of $In_{1-x}Ga_xP$ QDs synthesized in the bromide and iodide eutectics, and Figure 7d shows a similar comparison for the P 2p region, including data for the initial (DDA)₂S-capped InP QDs. In both cases, the In_{1-x}Ga_xP QDs synthesized in the iodide salt showed narrower peaks, which we ascribe to more homogeneous local coordination for the Ga and P atoms. These results support our hypothesis that the In_{1-x}Ga_xP QDs synthesized in the iodide medium have a more uniform alloy composition throughout the QD than In_{1-x}Ga_xP QDs synthesized in the bromide medium (Figure 7b). The alloyed In_{1-x}Ga_xP particles synthesized in an iodide medium are thus expected to have a more uniform gallium composition, and we expect that this more uniform composition yields the narrower ensemble emission spectra observed in these materials (Figure 6f).

A convolution of the $2p_{3/2}$ and $2p_{1/2}$ peaks at $\sim 128.1-128.8$ eV binding energies recorded in the P 2p region has been attributed to the predominant presence of a metal phosphide

(P³⁻) species in each sample.⁷⁶ Further, we noted the absence of any obvious signatures of oxidized phosphorous species at a higher binding energy (132–133 eV). Previous studies have related the presence of oxidized phosphorous species on the InP nanoparticle surface to the broadening of the emission spectra.^{74,75} The signal corresponding to the O 1s peak was very weak and corroborates this observation. XPS studies indicate that performing cation exchange reactions in halide molten salts enabled efficient protection of the nanocrystalline III—V phases from surface oxidation. The alkali halide molten salts not only show extraordinary temperature stability but can also efficiently prevent oxidation of III—V NCs.

CONCLUSIONS

We have shown that molten salt indium-to-gallium cation exchange is a dynamic system where the reaction can be tuned by changing several variables. The surface chemistry of the initial particles can be optimized to promote strong interactions with the salt matrix, enhancing colloidal stability, while the chemical composition of the surface can be chosen to stabilize the nanocrystalline phase. InP QDs can be well dispersed in a molten bromide eutectic with chalcogenide or metal halide ligands. We have shown that surface ligands play a role in the molten salt dispersal of InP QDs and impact further chemical reactions in this molten salt matrix. The surface chemistry for molten salt dispersal can likely be extended to other classes of inorganic ligands including halides and pseudohalides,³⁹ pnictides,⁷⁶ and chalcogenidometallates³⁸ as well as ligand-stripped particles.³⁷ We demonstrated that chalcogenide capping ligands form a chalcogen-rich shell which protects the InP QD phase at an elevated temperature. Future work will explore the optimization of surface ligands to achieve enhanced particle stability and improved fluorescence.

Time-dependent cation exchange experiments have shown that the reactions are kinetically limited under our experimental conditions. Expanding this cation exchange to further extremes of temperature and time may allow for the controlled synthesis of new In_{1-r}Ga_rP QD compositions. Overall, the InP to In_{1-x}Ga_xP cation exchange results achieved for InP QDs with a variety of initial surface chemistries prove the generality of the molten salt indium-to-gallium cation exchange synthetic method. By performing experiments spanning a vast swathe of the parameter space, we have made great strides toward achieving a narrow emission linewidth from a synthesis of alloyed III-V colloidal nanoparticles. We expect that the insights gained in this work may be used to demonstrate molten salt cation exchange with other III-V QDs (e.g., InAs, InSb), cation exchange with other ions (e.g. Al³⁺), and new synthetic manipulations of III-V QDs in molten salts (e.g. III-V core-shell synthesis). With our detailed experimentation and careful observations, we hope to contribute to the community's understanding of performing cation exchange reactions in colloidal III-V nanoparticles in molten inorganic salts. Equipped with the knowledge gained through our attempts at optimizing the alloyed core synthesis, we will be able to improve the optical performance of this system in the future.

ASSOCIATED CONTENT

Supporting Information

The Supporting Information is available free of charge at https://pubs.acs.org/doi/10.1021/acs.jpcc.1c10394.

Additional absorption and emission spectra, X-ray diffraction patterns and corresponding peak shifts, SAXS data, XPS spectra and photographs of the experimental setup (PDF).

AUTHOR INFORMATION

Corresponding Author

Dmitri V. Talapin — Department of Chemistry, James Franck Institute, and Pritzker School of Molecular Engineering, University of Chicago, Chicago, Illinois 60637, United States; Center for Nanoscale Materials, Argonne National Laboratory, Argonne, Illinois 60439, United States; orcid.org/0000-0002-6414-8587; Email: dvtalapin@uchicago.edu

Authors

Margaret H. Hudson – Department of Chemistry, James Franck Institute, and Pritzker School of Molecular Engineering, University of Chicago, Chicago, Illinois 60637, United States; Oorcid.org/0000-0002-8977-8139

Aritrajit Gupta — Department of Chemistry, James Franck Institute, and Pritzker School of Molecular Engineering, University of Chicago, Chicago, Illinois 60637, United States; orcid.org/0000-0001-9406-8986

Vishwas Srivastava — Department of Chemistry, James Franck Institute, and Pritzker School of Molecular Engineering, University of Chicago, Chicago, Illinois 60637, United States Eric M. Janke — Department of Chemistry, James Franck Institute, and Pritzker School of Molecular Engineering, University of Chicago, Chicago, Illinois 60637, United States

Complete contact information is available at: https://pubs.acs.org/10.1021/acs.jpcc.1c10394

Author Contributions

§M.H.H. and A.G. contributed equally.

Notes

The authors declare no competing financial interest.

ACKNOWLEDGMENTS

We thank Nanosys, Inc. (Milpitas, CA) for kindly providing colloidal InP QDs. The work on synthesis of ${\rm In_{1-x}Ga_xP}$ QDs was supported by the Samsung Global Research Outreach Program on New Materials. Advanced characterizations of colloidal dispersions in molten inorganic salts were supported by National Science Foundation under award number DMR-2004880. Spectroscopic studies of ${\rm In_{1-x}Ga_xP}$ QDs were funded by the Department of Defense (DOD) Air Force Office of Scientific Research under grant number FA9550-18-1-0099. This research used resources of the Center for Nanoscale Materials, a U.S. Department of Energy (DOE) Office of Science User Facility operated for the DOE Office of Science by Argonne National Laboratory under Contract no. DE-AC02-06CH11357.

■ REFERENCES

- (1) Coe-Sullivan, S.; Liu, W.; Allen, P.; Steckel, J. S. Quantum Dots for Led Downconversion in Display Applications. *ECS J. Solid State Sci. Technol.* **2013**, *2*, R3026–R3030.
- (2) Chen, H.; He, J.; Wu, S.-T. Recent Advances on Quantum-Dot-Enhanced Liquid-Crystal Displays. *IEEE J. Sel. Top. Quantum Electron.* **2017**, 23, 1–11.
- (3) Zhou, J.; Pu, C.; Jiao, T.; Hou, X.; Peng, X. A Two-Step Synthetic Strategy toward Monodisperse Colloidal CdSe and CdSe/

- CdS Core/Shell Nanocrystals. J. Am. Chem. Soc. 2016, 138, 6475-6483.
- (4) Chen, O.; et al. Compact High-Quality CdSe-CdS Core-Shell Nanocrystals with Narrow Emission Linewidths and suppressed Blinking. *Nat. Mater.* **2013**, *12*, 445-451.
- (5) Horn, D. A. In Eu Rohs Recast—New Requirements and Impacts for the Information and Communications Technology Industry. 2012 IEEE International Symposium on Sustainable Systems and Technology (ISSST), 16-18 May 2012. 2012; pp 1–5.
- (6) Das, A.; Snee, P. T. Synthetic Developments of Nontoxic Quantum Dots. *ChemPhysChem* **2016**, *17*, 598–617.
- (7) Park, J. P.; Lee, J.-J.; Kim, S.-W. Highly Luminescent InP/GaP/ZnS Qds Emitting in the Entire Color Range Via a Heating up Process. Sci. Rep. 2016, 6, 30094.
- (8) Xie, R.; Battaglia, D.; Peng, X. Colloidal InP Nanocrystals as Efficient Emitters Covering Blue to near-Infrared. *J. Am. Chem. Soc.* **2007**, *129*, 15432–15433.
- (9) Li, Y.; Hou, X.; Dai, X.; Yao, Z.; Lv, L.; Jin, Y.; Peng, X. Stoichiometry-Controlled InP-Based Quantum Dots: Synthesis, Photoluminescence, and Electroluminescence. *J. Am. Chem. Soc.* **2019**. *141*. 6448–6452.
- (10) Kim, Y.; Ham, S.; Jang, H.; Min, J. H.; Chung, H.; Lee, J.; Kim, D.; Jang, E. Bright and Uniform Green Light Emitting InP/ZnSe/ZnS Quantum Dots for Wide Color Gamut Displays. *ACS Appl. Nano Mater.* **2019**, *2*, 1496–1504.
- (11) Allen, P. M.; Walker, B. J.; Bawendi, M. G. Mechanistic Insights into the Formation of InP Quantum Dots. *Angew. Chem., Int. Ed.* **2010**, *49*, 760–762.
- (12) Gary, D. C.; Glassy, B. A.; Cossairt, B. M. Investigation of Indium Phosphide Quantum Dot Nucleation and Growth Utilizing Triarylsilylphosphine Precursors. *Chem. Mater.* **2014**, *26*, 1734–1744.
- (13) Stein, J. L.; Holden, W. M.; Venkatesh, A.; Mundy, M. E.; Rossini, A. J.; Seidler, G. T.; Cossairt, B. M. Probing Surface Defects of InP Quantum Dots Using Phosphorus $K\alpha$ and $K\beta$ X-Ray Emission Spectroscopy. *Chem. Mater.* **2018**, *30*, *6377*–*6388*.
- (14) Tessier, M. D.; Baquero, E. A.; Dupont, D.; Grigel, V.; Bladt, E.; Bals, S.; Coppel, Y.; Hens, Z.; Nayral, C.; Delpech, F. Interfacial Oxidation and Photoluminescence of InP-Based Core/Shell Quantum Dots. *Chem. Mater.* **2018**, *30*, 6877–6883.
- (15) Ramasamy, P.; Kim, N.; Kang, Y.-S.; Ramirez, O.; Lee, J.-S. Tunable, Bright, and Narrow-Band Luminescence from Colloidal Indium Phosphide Quantum Dots. *Chem. Mater.* **2017**, *29*, 6893–6899.
- (16) Ramasamy, P.; Ko, K.-J.; Kang, J.-W.; Lee, J.-S. Two-Step "Seed-Mediated" Synthetic Approach to Colloidal Indium Phosphide Quantum Dots with High-Purity Photo- and Electroluminescence. *Chem. Mater.* **2018**, *30*, 3643–3647.
- (17) Janke, E. M.; et al. Origin of Broad Emission Spectra in InP Quantum Dots: Contributions from Structural and Electronic Disorder. J. Am. Chem. Soc. 2018, 140, 15791–15803.
- (18) Kirkwood, N.; et al. Locating and Controlling the Zn Content in In(Zn)P Quantum Dots. *Chem. Mater.* **2020**, *32*, 557–565.
- (19) Fox, M.; Ispasoiu, R. Quantum Wells, Superlattices, and Band-Gap Engineering. Springer Handbook of Electronic and Photonic Materials; Springer, 2007; pp 1021–1040.
- (20) Kim, S.; et al. Highly Luminescent InP/GaP/ZnS Nanocrystals and Their Application to White Light-Emitting Diodes. *J. Am. Chem. Soc.* **2012**, *134*, 3804–3809.
- (21) Pietra, F.; Kirkwood, N.; De Trizio, L.; Hoekstra, A. W.; Kleibergen, L.; Renaud, N.; Koole, R.; Baesjou, P.; Manna, L.; Houtepen, A. J. Ga for Zn Cation Exchange Allows for Highly Luminescent and Photostable InZnP-Based Quantum Dots. *Chem. Mater.* **2017**, *29*, 5192–5199.
- (22) Srivastava, V.; Liu, W.; Janke, E. M.; Kamysbayev, V.; Filatov, A. S.; Sun, C.-J.; Lee, B.; Rajh, T.; Schaller, R. D.; Talapin, D. V. Understanding and Curing Structural Defects in Colloidal GaAs Nanocrystals. *Nano Lett.* **2017**, *17*, 2094–2101.
- (23) Srivastava, V.; Kamysbayev, V.; Hong, L.; Dunietz, E.; Klie, R. F.; Talapin, D. V. Colloidal Chemistry in Molten Salts: Synthesis of

- Luminescent $In_{1-x}Ga_xP$ and $In_{1-x}Ga_xAs$ Quantum Dots. *J. Am. Chem. Soc.* **2018**, *140*, 12144–12151.
- (24) Zhang, H.; Dasbiswas, K.; Ludwig, N. B.; Han, G.; Lee, B.; Vaikuntanathan, S.; Talapin, D. V. Stable Colloids in Molten Inorganic Salts. *Nature* **2017**, *542*, 328–331.
- (25) Kamysbayev, V.; Srivastava, V.; Ludwig, N. B.; Borkiewicz, O. J.; Zhang, H.; Ilavsky, J.; Lee, B.; Chapman, K. W.; Vaikuntanathan, S.; Talapin, D. V. Nanocrystals in Molten Salts and Ionic Liquids: Experimental Observation of Ionic Correlations Extending Beyond the Debye Length. *ACS Nano* **2019**, *13*, 5760–5770.
- (26) Dash, A.; Vaßen, R.; Guillon, O.; Gonzalez-Julian, J. Molten Salt Shielded Synthesis of Oxidation Prone Materials in Air. *Nat. Mater.* **2019**, *18*, 465–470.
- (27) Tmar, M.; Gabriel, A.; Chatillon, C.; Ansara, I. Critical Analysis and Optimization of the Thermodynamic Properties and Phase Diagrams in the III-V Compounds: The In-P and Ga-P Systems. *J. Cryst. Growth* **1984**, *68*, 557–580.
- (28) Fedorov, V. A.; Ganshin, V. A.; Korkishko, Y. N. Ion Exchange in II–VI Crystals: Thermodynamics, Kinetics, and Technology. *Phys. Status Solidi A* 1993, 139, 9–65.
- (29) Sundararaman, C. S.; Poulin, S.; Currie, J. F.; Leonelli, R. The Sulfur-Passivated InP Surface. *Can. J. Phys.* **1991**, *69*, 329–332.
- (30) Anderson, G. W.; Hanf, M. C.; Norton, P. R.; Lu, Z. H.; Graham, M. J. Thermal Stability of Sulfur Passivated InP(100)-(1×1). *Appl. Phys. Lett.* **1994**, *65*, 171–173.
- (31) Gallet, D.; Hollinger, G. Chemical, Structural, and Electronic Properties of Sulfur-Passivated InP(001) (2×1) Surfaces Treated with $(NH_4)_2S_x$. Appl. Phys. Lett. 1993, 62, 982–984.
- (32) Hazarika, A.; et al. Colloidal Atomic Layer Deposition with Stationary Reactant Phases Enables Precise Synthesis of "Digital" II—VI Nano-Heterostructures with Exquisite Control of Confinement and Strain. *J. Am. Chem. Soc.* **2019**, *141*, 13487–13496.
- (33) Beecher, A. N.; Yang, X.; Palmer, J. H.; LaGrassa, A. L.; Juhas, P.; Billinge, S. J. L.; Owen, J. S. Atomic Structures and Gram Scale Synthesis of Three Tetrahedral Quantum Dots. *J. Am. Chem. Soc.* **2014**, *136*, 10645–10653.
- (34) Nag, A.; Kovalenko, M. V.; Lee, J.-S.; Liu, W.; Spokoyny, B.; Talapin, D. V. Metal-Free Inorganic Ligands for Colloidal Nanocrystals: S²⁻, HS⁻, Se²⁻, HSe⁻, Te²⁻, HTe⁻, TeS₃²⁻, OH⁻, and NH₂⁻ as Surface Ligands. *J. Am. Chem. Soc.* **2011**, *133*, 10612–10620.
- (35) Dirin, D. N.; Dreyfuss, S.; Bodnarchuk, M. I.; Nedelcu, G.; Papagiorgis, P.; Itskos, G.; Kovalenko, M. V. Lead Halide Perovskites and Other Metal Halide Complexes as Inorganic Capping Ligands for Colloidal Nanocrystals. *J. Am. Chem. Soc.* **2014**, *136*, 6550–6553.
- (36) Ilavsky, J.; Jemian, P. R. Irena: Tool Suite for Modeling and Analysis of Small-Angle Scattering. *J. Appl. Crystallogr.* **2009**, 42, 347–353
- (37) Rosen, E. L.; Buonsanti, R.; Llordes, A.; Sawvel, A. M.; Milliron, D. J.; Helms, B. A. Exceptionally Mild Reactive Stripping of Native Ligands from Nanocrystal Surfaces by Using Meerwein's Salt. *Angew. Chem., Int. Ed.* **2012**, *51*, 684–689.
- (38) Kovalenko, M. V.; Scheele, M.; Talapin, D. V. Colloidal Nanocrystals with Molecular Metal Chalcogenide Surface Ligands. *Science* **2009**, 324, 1417–1420.
- (39) Zhang, H.; Jang, J.; Liu, W.; Talapin, D. V. Colloidal Nanocrystals with Inorganic Halide, Pseudohalide, and Halometallate Ligands. *ACS Nano* **2014**, *8*, 7359–7369.
- (40) Bessolov, V. N.; Lebedev, M. V. Chalcogenide Passivation of III–V Semiconductor Surfaces. *Semiconductors* **1998**, 32, 1141–1156.
- (41) Tessier, M. D.; Dupont, D.; De Nolf, K.; De Roo, J.; Hens, Z. Economic and Size-Tunable Synthesis of InP/ZnE (E = S, Se) Colloidal Quantum Dots. *Chem. Mater.* **2015**, 27, 4893–4898.
- (42) Fisher, D. J. Diffusion in Semiconductors, Other Than Silicon: Compilation; Trans Tech, 2010.
- (43) Scalise, E.; Srivastava, V.; Janke, E.; Talapin, D.; Galli, G.; Wippermann, S. Surface Chemistry and Buried Interfaces in All-Inorganic Nanocrystalline Solids. *Nat. Nanotechnol.* **2018**, *13*, 841–848.

- (44) Van Orman, J. A.; Grove, T. L.; Shimizu, N. Rare Earth Element Diffusion in Diopside: Influence of Temperature, Pressure, and Ionic Radius, and an Elastic Model for Diffusion in Silicates. *Contrib. Mineral. Petrol.* **2001**, *141*, 687–703.
- (45) Ithurria, S.; Talapin, D. V. Colloidal Atomic Layer Deposition (c-Ald) Using Self-Limiting Reactions at Nanocrystal Surface Coupled to Phase Transfer between Polar and Nonpolar Media. *J. Am. Chem. Soc.* **2012**, *134*, 18585–18590.
- (46) Kovalenko, M. V.; Bodnarchuk, M. I.; Talapin, D. V. Nanocrystal Superlattices with Thermally Degradable Hybrid Inorganic-Organic Capping Ligands. J. Am. Chem. Soc. 2010, 132, 15124–15126.
- (47) Janz, G. J.; Allen, C. B.; Downey, J. R.; Tomkins, R. P. T. Physical Properties Data Compilations Relevant to Energy Storage. I. Molten Salts: Eutectic Data. *Nat. Bur. Stand.* 1978, 244.
- (48) Tsui, E. Y.; Hartstein, K. H.; Gamelin, D. R. Selenium Redox Reactivity on Colloidal CdSe Quantum Dot Surfaces. *J. Am. Chem. Soc.* **2016**, *138*, 11105–11108.
- (49) Kim, T.-G.; Zherebetskyy, D.; Bekenstein, Y.; Oh, M. H.; Wang, L.-W.; Jang, E.; Alivisatos, A. P. Trap Passivation in Indium-Based Quantum Dots through Surface Fluorination: Mechanism and Applications. *ACS Nano* **2018**, *12*, 11529–11540.
- (50) Liu, W.; Lee, J.-S.; Talapin, D. V. III-V Nanocrystals Capped with Molecular Metal Chalcogenide Ligands: High Electron Mobility and Ambipolar Photoresponse. *J. Am. Chem. Soc.* **2013**, *135*, 1349–1357.
- (51) Jang, J.; Liu, W.; Son, J. S.; Talapin, D. V. Temperature-Dependent Hall and Field-Effect Mobility in Strongly Coupled All-Inorganic Nanocrystal Arrays. *Nano Lett.* **2014**, *14*, 653–662.
- (52) Riesz, F.; Dobos, L.; Vignali, C.; Pelosi, C. Thermal Decomposition of InP Surfaces: Volatile Component Loss, Morphological Changes, and Pattern Formation. *J. Mater. Sci. Eng. B* **2001**, *80*, 54–59.
- (53) Tsang, W. T. Semiconductors and Semimetals; Elsevier Science, 1985.
- (54) Borisenko, V. E.; Hesketh, P. J. Rapid Thermal Processing of Semiconductors; Springer US, 2013.
- (55) Chen, K. Y.; Morris, J. C. Kinetics of Oxidation of Aqueous Sulfide by Oxygen. *Environ. Sci. Technol.* **1972**, *6*, 529–537.
- (56) Everett, D. H. Manual of Symbols and Terminology for Physicochemical Quantities and Units, Appendix II: Definitions, Terminology and Symbols in Colloid and Surface Chemistry. *Pure Appl. Chem.* **1972**, *31*, 577.
- (57) Foyt, A. G. The Electro-Optic Applications of InP. J. Cryst. Growth 1981, 54, 1–8.
- (58) Li, T.; Senesi, A. J.; Lee, B. Small Angle X-Ray Scattering for Nanoparticle Research. *Chem. Rev.* **2016**, *116*, 11128–11180.
- (59) Ma, X.; Min, J.; Zeng, Z.; Garoufalis, C. S.; Baskoutas, S.; Jia, Y.; Du, Z. Excitons in InP, GaP, and Ga_xIn_{1-x}P Quantum Dots: Insights from Time-Dependent Density Functional Theory. *Phys. Rev. B* **2019**, *100*, 245404.
- (60) Morrison, C.; Sun, H.; Yao, Y.; Loomis, R. A.; Buhro, W. E. Methods for the ICP-OES Analysis of Semiconductor Materials. *Chem. Mater.* **2020**, 32, 1760–1768.
- (61) Jana, S.; de Frutos, M.; Davidson, P.; Abécassis, B. Ligand-Induced Twisting of Nanoplatelets and Their Self-Assembly into Chiral Ribbons. *Sci. Adv.* **2017**, *3*, No. e1701483.
- (62) Zhou, Y.; Wang, F.; Buhro, W. E. Large Exciton Energy Shifts by Reversible Surface Exchange in 2D II-VI Nanocrystals. *J. Am. Chem. Soc.* **2015**, *137*, 15198–15208.
- (63) Meulenberg, R. W.; Jennings, T.; Strouse, G. F. Compressive and Tensile Stress in Colloidal CdSe Semiconductor Quantum Dots. *Phys. Rev. B: Condens. Matter Mater. Phys.* **2004**, *70*, 235311.
- (64) Goldstein, B. Diffusion in Compound Semiconductors. *Phys. Rev.* 1961, 121, 1305–1311.
- (65) Nelson, A.; Honrao, S.; Hennig, R. G.; Robinson, R. D. Nanocrystal Symmetry Breaking and Accelerated Solid-State Diffusion in the Lead—Cadmium Sulfide Cation Exchange System. *Chem. Mater.* **2019**, *31*, 991–1005.

- (66) Ovid'ko, I. A. Deformation and Diffusion Modes in Nanocrystalline Materials. *Int. Mater. Rev.* **2005**, *50*, 65–82.
- (67) Bublik, V. T.; Leikin, V. N. Calculation of the Pseudobinary Alloy Semiconductor Phase Diagrams. *Phys. Status Solidi A* **1978**, 46, 365–372.
- (68) Mićić, O. I.; Sprague, J.; Lu, Z.; Nozik, A. J. Highly Efficient Band-Edge Emission from InP Quantum Dots. *Appl. Phys. Lett.* **1996**, 68, 3150–3152.
- (69) Talapin, D. V.; Gaponik, N.; Borchert, H.; Rogach, A. L.; Haase, M.; Weller, H. Etching of Colloidal InP Nanocrystals with Fluorides:Photochemical Nature of the Process Resulting in High Photoluminescence Efficiency. *J. Phys. Chem. B* **2002**, *106*, 12659–12663.
- (70) Houtepen, A. J.; Hens, Z.; Owen, J. S.; Infante, I. On the Origin of Surface Traps in Colloidal II–VI Semiconductor Nanocrystals. *Chem. Mater.* **2017**, *29*, 752–761.
- (71) Busby, E.; Anderson, N. C.; Owen, J. S.; Sfeir, M. Y. Effect of Surface Stoichiometry on Blinking and Hole Trapping Dynamics in CdSe Nanocrystals. *J. Phys. Chem. C* **2015**, *119*, 27797–27803.
- (72) Hughes, K. E.; Stein, J. L.; Friedfeld, M. R.; Cossairt, B. M.; Gamelin, D. R. Effects of Surface Chemistry on the Photophysics of Colloidal InP Nanocrystals. *ACS Nano* **2019**, *13*, 14198–14207.
- (73) Stein, J. L.; Mader, E. A.; Cossairt, B. M. Luminescent InP Quantum Dots with Tunable Emission by Post-Synthetic Modification with Lewis Acids. *J. Phys. Chem. Lett.* **2016**, *7*, 1315–1320.
- (74) Clearfield, A. Role of Ion Exchange in Solid-State Chemistry. *Chem. Rev.* **1988**, 88, 125–148.
- (75) Schlesinger, M. E. The Thermodynamic Properties of Phosphorus and Solid Binary Phosphides. *Chem. Rev.* **2002**, *102*, 4267–4302.
- (76) Ban, H. W.; Oh, J. G.; Jo, S.; Jeong, H.; Gu, D. H.; Baek, S.; Lee, S. Y.; Park, Y. I.; Jang, J.; Son, J. S. Polyphosphide Precursor for Low-Temperature Solution-Processed Fibrous Phosphorus Thin Films. *Chem. Mater.* **2019**, *31*, 5909–5918.

□ Recommended by ACS

Seeded Growth of HgTe Nanocrystals for Shape Control and Their Use in Narrow Infrared Electroluminescence

Yoann Prado, Emmanuel Lhuillier, et al.

MARCH 12, 2021

CHEMISTRY OF MATERIALS

READ 🗹

Roll-To-Roll Friendly Solution-Processing of Ultrathin, Sintered CdTe Nanocrystal Photovoltaics

J. Matthew Kurley, Dmitri V. Talapin, et al.

SEPTEMBER 08, 2021

ACS APPLIED MATERIALS & INTERFACES

READ 🗹

Synthesis of Wurtzite In and Ga Phosphide Quantum Dots Through Cation Exchange Reactions

Xinyao Shan, Botao Ji, et al.

JUNE 22, 2021

CHEMISTRY OF MATERIALS

READ 🗹

Continuous Nucleation and Size Dependent Growth Kinetics of Indium Phosphide Nanocrystals

Brandon M. McMurtry, Jonathan S. Owen, et al.

MAY 06, 2020

CHEMISTRY OF MATERIALS

READ 🗹

Get More Suggestions >